

---

## Disclaimer

---

This manuscript is under review in NATURE COMMUNICATIONS EARTH & ENVIRONMENT. Please note that the MS has not undergone peer review at this stage. Subsequent versions of this manuscript may have different content. If accepted, the final version of this manuscript will be available via the 'Peer-reviewed Publication DOI' link on the right-hand side of this webpage. Please feel free to contact any of the authors with feedback and suggestions for improvements.

### Document history

---

Date	Action
1/Jul/2020	MS sent to co-authors for final draft acceptance
3/Jul/2020	IGSN for samples requested Spreadsheet and scripts submitted to Zenodo MS Submitted to EarthArXiv
8/Jul/2020	Preprint DOI Received MS Submitted to Nature Geoscience
14/Jul/2020	IGSN received and inserted for all samples Small style adjustments to tables
21/Jul/2020	Received initial decision from Nature Geoscience Transferred to Nature Communications
29/Jul/2020	Sent to reviewers by Nature Communications
3/Sept/2020	Reviews received, pending transfer to other journal
15/Oct/2020	Scripts and data updated in Zenodo, last check by first author
21/Oct/2020	Reviews completed, paper transferred to Communications Earth and Environment with answer to reviewers comments
3/Nov/2020	Revised version uploaded to EarthArxiv Title has been updated as per journal editorial team request

---

# HIGHER THAN PRESENT GLOBAL MEAN SEA LEVEL RECORDED BY AN EARLY PLIOCENE INTERTIDAL UNIT IN PATAGONIA (ARGENTINA).

PREPRINT, COMPILED NOVEMBER 11, 2020

Alessio Rovere<sup>1</sup>, Marta Pappalardo<sup>2</sup>, Sebastian Richiano<sup>3</sup>, Marina Aguirre<sup>4,5</sup>, Michael R. Sandstrom<sup>6</sup>, Paul J. Hearty<sup>7</sup>, Jacqueline Austermann<sup>6</sup>, Ignacio Castellanos<sup>5</sup>, and Maureen E. Raymo<sup>6</sup>

<sup>1</sup>MARUM - Center for Marine Environmental Sciences, University of Bremen. Leobener Str. 8., D-28359, Bremen, Germany

<sup>2</sup>Department of Earth Sciences, Università degli studi di Pisa. Via S. Maria 53, 56126, Pisa Italy

<sup>3</sup>Instituto Patagónico de Geología y Paleontología, CONICET. Bv. Almirante Brown 2915, Puerto Madryn (9120), Chubut, Argentina

<sup>4</sup>CONICET, CCT-La Plata and Universidad Nacional de La Plata. Calle 8 n.1467, B1904CMC, La Plata, Buenos Aires, Argentina

<sup>5</sup>Facultad de Ciencias Naturales y Museo, Universidad Nacional de La Plata. Calle 64 n.3, 1900 La Plata, Buenos Aires, Argentina

<sup>6</sup>Lamont Doherty Earth Observatory, Columbia University. 61 Rte 9W, Palisades, NY 10964, United States

<sup>7</sup>Department of Geological Sciences, Jackson School of Geosciences, The University of Texas at Austin. 2275 Speedway Stop C9000, Austin, Texas, United States

## ABSTRACT

Reconstructions of global mean sea level from earlier warm periods in Earth's history can help constrain future projections of sea level rise. Here we report on the sedimentology and age of a geological unit in central Patagonia, Argentina, that we dated to the Early Pliocene (4.69-5.23 Ma,  $2\sigma$ ) with strontium isotope stratigraphy. The unit was interpreted as representative of an intertidal environment, and its elevation was measured with differential GPS at ca. 36 m above present-day sea level. Considering modern tidal ranges, it was possible to constrain paleo relative sea level within  $\pm 2.7\text{m}$  ( $1\sigma$ ). We use glacial isostatic adjustment models and estimates of vertical land movement to calculate that, when the Camarones intertidal sequence was deposited, global mean sea level was  $28.4 \pm 11.7\text{m}$  ( $1\sigma$ ) above present. This estimate matches those derived from analogous Early Pliocene sea level proxies in the Mediterranean Sea and South Africa. Evidence from these three locations indicates that Early Pliocene sea level may have exceeded 20m above its present level. Such high global mean sea level values imply an ice-free Greenland, a significant melting of West Antarctica, and a contribution of marine-based sectors of East Antarctica to global mean sea level.

**Keywords** Early Pliocene · Sea level · Stratigraphy

## 1 INTRODUCTION

2 The survey, interpretation and dating of paleo relative sea level  
3 (RSL) indicators (such as fossil coral reefs or relic beach de-  
4 posits<sup>1</sup>) is paramount to constraining the maximum elevation  
5 reached by global mean sea level during periods of the Earth's  
6 history warmer than the pre-industrial. The elevation of paleo  
7 RSL indicators is the only direct proxy available to estimate  
8 global mean sea level in Earth's past. Once measured, observed  
9 paleo RSL indicators must be corrected for processes causing  
10 "Departures from Eustasy"<sup>2</sup> (such as tectonics, mantle dynamic  
11 topography, DT, and glacial isostatic adjustment, GIA<sup>3;4</sup>) to  
12 obtain paleo global mean sea level (GMSL) estimates. These  
13 are in turn important to informing models of ice sheet melting  
14 under future warmer climates<sup>5</sup>.

15 A recent global database<sup>6</sup> shows that about 5000 RSL indica-  
16 tors were preserved since the Last Glacial Maximum (30 ka).  
17 Well-preserved and dated RSL indicators are relatively rare for  
18 older time periods: another compilation of Pleistocene RSL in-  
19 dicators<sup>7</sup> reports more than 1000 Last Interglacial (MIS 5e, 125  
20 ka) and only around 20 MIS 11 (400 ka) RSL indicators. Only a  
21 handful of sites exist that document sea level highstands beyond  
22 one million years ago<sup>2;8;9;10;11</sup>. In general, robust RSL indica-  
23 tors predating 400 ka are rare to find because they are poorly  
24 preserved and are most often difficult to date with precision.  
25 Additionally, relating them to GMSL is difficult since they are

likely affected by significant post-depositional movements. This  
limits our ability to gauge the sensitivity of ice caps to warmer  
climate conditions, such as those that characterized Earth in the  
Pliocene.

Some of the oldest, precisely dated and measured RSL indicators  
were recently reported on the island of Mallorca (Balearic Is-  
lands, Spain), in a coastal cave called "Coves d'Artá". Here, six  
phreatic overgrowths on speleothems mark the paleo water/air  
interface within the cave<sup>9</sup>, and are therefore closely related to  
paleo RSL. The highest and oldest of these formations was mea-  
sured at  $31.8 \pm 0.25\text{m}$  above mean sea level, and yielded a U-Pb  
age of  $4.29 \pm 0.39\text{Ma}$  ( $2\sigma$ )<sup>9</sup>. Taking into account GIA and  
possible long-term deformation due to tectonics or dynamic to-  
pography, it was estimated that global mean sea level at the time  
of deposition of this RSL indicator was 25.1m above present,  
bounded by uncertainties represented by 16<sup>th</sup>-84<sup>th</sup> percentiles  
of 10.6-28.3m<sup>9</sup>. For the same time period, a second study<sup>10</sup>  
reported a site in the Republic of South Africa (Northern Cape  
Province, site Cliff Point-ZCP Section2). Here, oyster shells liv-  
ing in a paleo subtidal to intertidal environment constrain paleo  
RSL at  $35.1 \pm 2.2\text{m}$  ( $1\sigma$ ). The oysters were dated to 4.28-4.87  
Ma ( $2\sigma$  range) with strontium isotope stratigraphy (SIS). While  
paleo global mean sea level estimates were not calculated at  
this site, based on the Mallorca benchmark the authors argue

26  
27  
28  
29  
30  
31  
32  
33  
34  
35  
36  
37  
38  
39  
40  
41  
42  
43  
44  
45  
46  
47  
48  
49

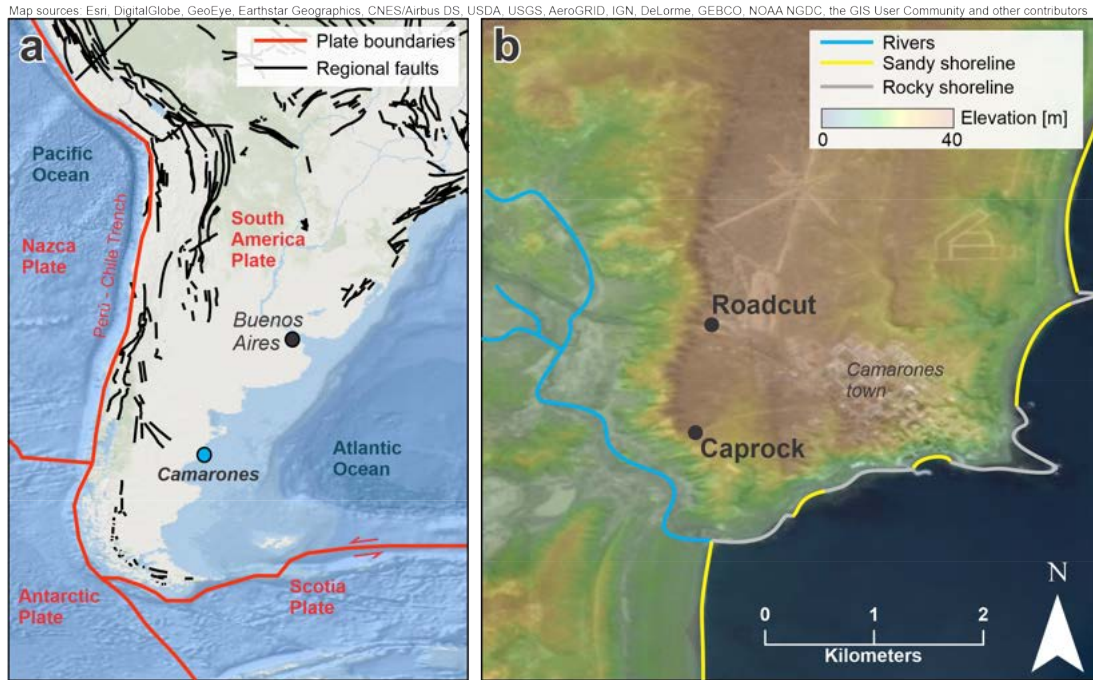


Figure 1: General and specific location of the study area. **a)** Location of the study area and main geological structures in the Southern part of South America. **b)** Topography of the Camarones town area, with location of the two outcrops (*Roadcut* and *Caprock*) presented in this study. Map sources: Esri, DigitalGlobe, GeoEye, Earthstar Geographics, CNES/Airbus DS, USDA, USGS, AeroGRID, IGN, DeLorme, GEBCO, NOAA NGDC, SRTM, the GIS User Community and other contributors. Elevation data in B are from the Shuttle Radar Topography Mission<sup>12</sup>.

50 that this location was affected by relatively minor vertical land  
51 movements (possibly uplift) since 5 Ma.

52 While indirect paleo sea level estimates spanning the last 5.3 Ma  
53 are available from oxygen isotopes<sup>13;14;15</sup>, the two studies cited  
54 above are arguably the only ones reporting relatively precise and  
55 well-dated direct sea-level observations for the Early Pliocene,  
56 that is regarded as a past analogue for future warmer climate<sup>16</sup>.  
57 At this time, CO<sub>2</sub> was between pre-industrial and modern levels,  
58 with possibly higher peaks to 450 ppm<sup>17;16</sup>. During Early  
59 Pliocene interglacials, average global temperatures were 2-3°C  
60 higher than pre-industrial values<sup>18;16</sup>. Pliocene climate was  
61 modulated by a ca. 40 kyr periodicity in glacial/interglacial  
62 cycles with highstands and lowstands that were characterized by  
63 sea-level oscillations as high as 13 ± 5m<sup>19</sup>. Ice models suggest  
64 that, during the warmest Pliocene interglacials, Greenland was  
65 ice-free<sup>20</sup>. Similarly, they suggest that the West Antarctic Ice  
66 sheet was likely subject to periodic collapses<sup>21</sup>, and might have  
67 contributed as much as 7m<sup>22</sup> to GMSL. Ice models and field-  
68 based evidence<sup>23</sup> suggest that also the East Antarctic Ice Sheet  
69 might have been smaller than today, contributing another 3m<sup>22</sup>  
70 to 13-16m<sup>24</sup> to GMSL.

71 In this study, we report a foreshore (intertidal) sequence located  
72 in the town of Camarones, along the coast of central Patagonia,  
73 Argentina (Figure 1). Combining field data, SIS ages, GIA and  
74 DT models we conclude that this deposit formed 4.69-5.23Ma  
75 ago (2σ range) when sea level was 28.4 ± 11.7 (1σ) higher than  
76 today. This estimate is broadly consistent with those derived  
77 from the Republic of South Africa and Spain. Together,  
78 these three studies present a coherent picture of global mean sea

level during the Early Pliocene, that likely exceeded 20m above  
modern sea level.

### STUDY AREA: CAMARONES, CENTRAL PATAGONIA, ARGENTINA

The Patagonia geographic region includes territories belonging to the states of Argentina and Chile. Geologically, Patagonia represents the southernmost tip of the South American plate (Figure 1a). Along the Pacific coasts of Patagonia, the Nazca and the Antarctic plates are subducting below the Andes. Towards the south, the Scotia plate moves eastward and outlines Tierra del Fuego, at South America's southern tip<sup>25</sup>. To the East, the Patagonian Atlantic coast is a passive margin, tectonically characterized as an extensional stress field and bordered by a wide continental shelf. The central and eastern parts of this landmass are represented by the Andean foreland, formed by a Palaeozoic-Mesozoic metamorphic basement overlapped by Tertiary continental and marine sedimentary rocks, dating back to the Paleocene. These are covered by Eocene–Oligocene pyroclastic rocks and Middle Miocene fluvial sediments. Marine sedimentary rocks corresponding to Tertiary transgressions are located east of the Andean foreland<sup>26</sup>. In the Middle Miocene, the Chile Triple Junction migrated northward, leading to the opening of an asthenospheric window below southern Patagonia<sup>27</sup>. This caused a switch from subsidence to uplift, and the Patagonia region underwent a moderate but continuous uplift.<sup>28</sup>

Along the coastlines of Central Patagonia, several levels of paleo shorelines above modern sea level were noted by Charles Darwin

79  
80  
81  
82  
83  
84  
85  
86  
87  
88  
89  
90  
91  
92  
93  
94  
95  
96  
97  
98  
99  
100  
101  
102  
103  
104  
105



Figure 2: The *Roadcut* outcrop at Camarones. The inset shows a detail of Unit **Cp**, a shelly-rich layer interpreted as representative of a foreshore (intertidal) environment dating to the Early Pliocene. Each unit is described in details in the Supplementary Note 2, including descriptions of the *Caprock* outcrop.

106 in his Beagle voyage<sup>29</sup>, and were the subject of more than 150  
 107 years of research (See Supplementary Note 1 and Supplementary  
 108 Table 1). Studies of Pleistocene coastal sequences in Central  
 109 Patagonia include outcrops of Holocene<sup>30;31</sup>, Pleistocene<sup>32;33;34</sup>  
 110 and Pliocene-to-Miocene<sup>35;36</sup> age. Among the latter, Del Río et  
 111 al. (2013)<sup>36</sup> dated Early Pliocene mollusks from marine deposits  
 112 few hundreds of kilometers south of the study area described in  
 113 this study.

114 The town of Camarones lies at the northern tip of the San Jorge  
 115 Gulf, approximately 1300 km south of Buenos Aires. Within a  
 116 few kilometers of Camarones, several paleo-sea level indicators  
 117 have been preserved, from the Holocene<sup>37</sup> to the Pleistocene<sup>32</sup>.  
 118 Already in the late 1940s, the Italian geologist Feruglio<sup>38</sup> iden-  
 119 tified an elevated marine terrace along a roadcut carved on the  
 120 main road leading into the town of Camarones that he tenta-  
 121 tively attributed to the Pliocene. He called this terrace, the  
 122 Camarones High Terrace (originally, in Spanish, *Teraza Alta de*  
 123 *Camarones*<sup>38</sup>). A recent study<sup>32</sup> confirmed the elevation of the  
 124 Camarones High Terrace at ca. 40m above sea level, at the lower  
 125 bound of the "beach barriers and terrace deposits between 40  
 126 and 110m elevation" reported by the 1:250.000 geological chart  
 127 of Camarones<sup>39</sup>.

## 128 RESULTS: THE PLIOCENE SEA LEVEL RECORD AT 129 CAMARONES AND GMSL ESTIMATES

130 Radiometric ages, precise GPS elevations and stratigraphic de-  
 131 scriptions of cross-sections surveyed along the Camarones High  
 132 Terrace are the subject of this paper. Along this terrace, we  
 133 surveyed and dated samples from two sites, separated by less  
 134 than one kilometer. One is the *Roadcut*, already recognized  
 135 and described by Feruglio<sup>38</sup>. We did not find reports of the

second site (that we here call *Caprock*, Figure 1b) in the exist-  
 ing literature, although it is possible that it was included in the  
 geological description of the High Terrace by previous authors.  
 At both sites, we recognized a geological facies representative  
 of sedimentation in a foreshore environment (i.e. in the inter-  
 tidal zone) that marks paleo RSL with high accuracy. All data  
 described hereafter and in Supplementary Note 2 is available in  
 spreadsheet form from Rovere et al. (2020)<sup>40</sup>

**Paleo RSL.** In general, *Roadcut* and *Caprock* represent sedi-  
 mentation during a transgressive event on top of a raised shore  
 platform (Supplementary Figure 1-2). Among the units iden-  
 tified within the *Roadcut* (Figure 2), one (Unit **Cp**, see inset  
 in Figure 2) is composed of well-cemented fine conglomerates  
 with rounded pebbles and shells. In particular, the uppermost  
 part of this unit contains a dense faunal assemblage in the form  
 of a shellbed, where we recognized 15 different species of bi-  
 valves and 11 species of gastropods (Supplementary Table 2).  
 The bivalve shells are mostly intact and sometimes with paired  
 valves (articulated), but not in living position. This unit was  
 interpreted as representative of a foreshore environment, i.e. the  
 intertidal zone. The same unit has been identified at the *Caprock*  
 section, at roughly the same elevation. The elevation of Unit  
**Cp** was measured at two points at both *Roadcut* and *Caprock*  
 (Table 1). From these measurements, we calculate that Unit  
**Cp** has an **average elevation of  $36.2 \pm 0.9\text{m}$  ( $1\sigma$ )** above the  
 GEOIDEAR16 geoid<sup>41</sup>, which is the best approximation for  
 present sea level in Argentina. Using modern tidal values<sup>37</sup>,  
 and assuming no post-depositional movement, we calculate that  
 the two outcrops in the area of Camarones are indicative of a  
**paleo RSL at  $36.2 \pm 2.7\text{m}$  ( $1\sigma$ )** above present (see Methods for  
 details).

167 **Age.** Three oyster shells from *Roadcut* and *Caprock* were  
 168 analyzed by strontium isotope stratigraphy (SIS) relative dating  
 169 techniques. Using sequential leaching to target the least altered  
 170 inner carbonate of each shell, we obtained multiple SIS ages on  
 171 three different shells (one from *Caprock* and two from *Roadcut*;  
 172 see Sandstrom et al., 2020<sup>11</sup> for a detailed description of the  
 173 adopted methodology). The shells yielded an age range of **4.69–**  
 174 **5.23Ma** ( $n=6$ ,  $2\sigma$   $S_{EM}$ ).

175 **Glacial Isostatic Adjustment.** The Early Pliocene intertidal  
 176 units surveyed at Camarones were subject to processes that  
 177 caused their past and current elevation to depart from GMSL.  
 178 These include glacial isostatic adjustment (GIA) and other verti-  
 179 cal land motions (VLMs). We calculate GIA using 36 different  
 180 Earth models. For this site, we calculate a GIA correction of  
 181  $-14.6 \pm 3.2\text{m}$  ( $1\sigma$ ) (see Methods for details). This value is  
 182 subtracted from the observed paleo RSL and the uncertainty  
 183 propagated. This correction is a combination of effects associ-  
 184 ated with i) the ongoing response to the last deglaciation, and ii)  
 185 Antarctic ice sheet oscillations during the early Pliocene<sup>2</sup>. The  
 186 former contribution is  $-9.5 \pm 3\text{m}$  ( $1\sigma$ ), which means that the  
 187 Argentinian coast today experiences sea level fall due to a combi-  
 188 nation of effects associated with postglacial rebound due to the  
 189 melting of the glacial Patagonian ice sheet as well as continental  
 190 levering, ocean syphoning, and rotational effects. Once fully  
 191 relaxed, sea level at Camarones will therefore be lower (and a  
 192 paleo sea level indicator higher) by approximately 9.5m than  
 193 it is today. The additional contribution of  $\sim -5\text{m}$  is associated  
 194 with the adjustment to 40kyr oscillations in the Antarctic ice  
 195 sheet. The result is that, at Camarones, **GIA-corrected paleo**  
 196 **RSL is  $50.8 \pm 4.2\text{m}$**  ( $1\sigma$ ).

197 **Vertical Land Motions.** The GIA-corrected RSL elevation re-  
 198 ported above needs to be further corrected for VLMs, that can be  
 199 either due to crustal tectonics, mantle dynamic topography<sup>42;43</sup>  
 200 or deformation associated with sediment loading/unloading<sup>44;45</sup>.  
 201 As briefly outlined in the previous sections, Camarones is lo-  
 202 cated on a passive margin, likely subject to limited tectonic  
 203 influence. Dynamic topography models suggest that, since MIS  
 204 5e (125 ka), the area of Camarones was subject to uplift, with  
 205 rates increasing towards the South<sup>3</sup>. This is in line with obser-  
 206 vations of much higher Pliocene shorelines (70–170m above sea  
 207 level<sup>36</sup>) at locations 300–500 kilometers south of Camarones  
 208 (Supplementary Note 1). A long-term slight uplift trend is also  
 209 predicted by the models of Flament et al. (2015)<sup>46</sup> and Müller  
 210 et al. (2018)<sup>47</sup>. Predictions in these DT models average to  
 211  $4.5 \pm 2.2\text{m/Ma}$  (Table 3). Accounting for the age of the deposit  
 212 (including  $1\sigma$  uncertainties), this leads to a downward correc-  
 213 tion of our global mean sea level inference by  $22.4 \pm 11.0\text{m}$   
 214 ( $1\sigma$ ). As is apparent from the variation of estimates for the dy-  
 215 namic topography rate, this correction remains quite uncertain  
 216 and the true value can possibly be even outside of this range  
 217 given that it is difficult to fully explore model uncertainties (see  
 218 Discussion section).

219 **Global Mean Sea Level.** Using the value of VLM reported  
 220 above and propagating the uncertainties related to RSL, GIA  
 221 and VLM, we calculate that, at the time of deposition of the  
 222 *Caprock* and *Roadcut* outcrops, **GMSL was  $28.4 \pm 11.7\text{m}$**  ( $1\sigma$ )  
 223 . We remark that there are large unknowns associated with this  
 224 value. First, as described above, dynamic topography remains a

process that has high uncertainties that are generally not fully  
 quantified. Second, it is possible that, as it is the case for the US  
 Atlantic Coastal Plain<sup>44</sup>, flexural response to sediment loading  
 or tectonic deformation (that are not considered here) could also  
 contribute to further vertical land motions in this area.

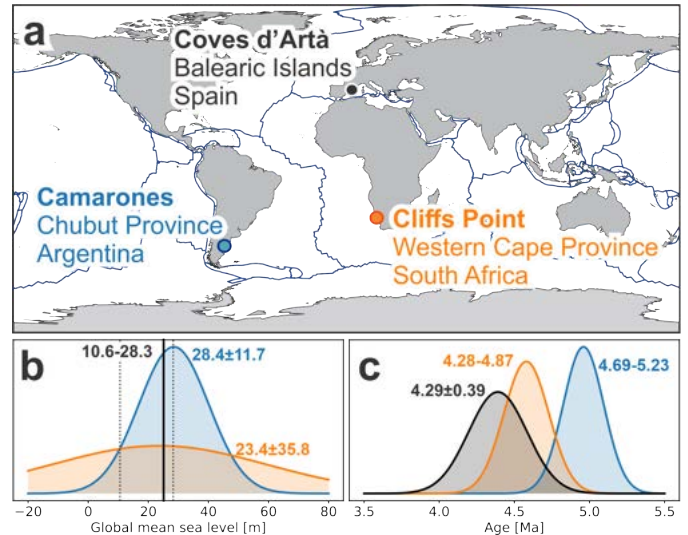


Figure 3: Comparison among Early Pliocene sea level stratigraphic reconstructions. **a)** Location of Early Pliocene RSL indicators discussed in the text. Plate boundaries are shown in dark blue for reference<sup>48</sup>. **b)** Global Mean Sea Level (GMSL) estimates for: i) Coves d'Artà (Balearic Islands, Spain), solid black line represents the most likely value (25.1m), dotted black lines the 16<sup>th</sup> and 84<sup>th</sup> percentiles<sup>9</sup>; ii) Camarones, Argentina (blue gaussian); iii) Cliffs Point, South Africa (orange gaussian, calculated from data in Hearty et al. (2020)<sup>10</sup>, corrected with the same GIA and subset of applicable DT models used for Camarones. **c)** Age estimates for Coves d'Artà (black), Camarones (blue) and Cliffs Point (orange).

## DISCUSSION: EARLY PLIOCENE GLOBAL MEAN SEA LEVEL

Our results show that the intertidal units at Camarones are of Early Pliocene age (4.69–5.23Ma,  $2\sigma$   $S_{EM}$ ). The sedimentological and stratigraphic characteristics of the deposits analysed in this study lead to the conclusion that they formed during a sea level highstand, when GMSL was  $28.4 \pm 11.7\text{m}$  ( $1\sigma$ ) higher than present. We note that there are still large uncertainties on this GMSL estimate, which derive mostly from vertical land motion corrections, stemming from the variability of published dynamic topography predictions<sup>46;47</sup>. Exploring and reducing these uncertainties requires improved mapping of the mantle structure beneath Patagonia from seismic tomography, a better understanding of how wave speeds map into density variations, and improved constraints on the rheology of the subsurface. Recent advances tackle these shortcomings and promise to reduce uncertainties in the estimate of vertical land motion<sup>57;58</sup>. Another strategy to investigate vertical land motions at Camarones would be to use the Pleistocene shorelines at the same site to extract a long-term uplift rate for the area. We argue that such approach would lead to similarly large error bars due to uncer-

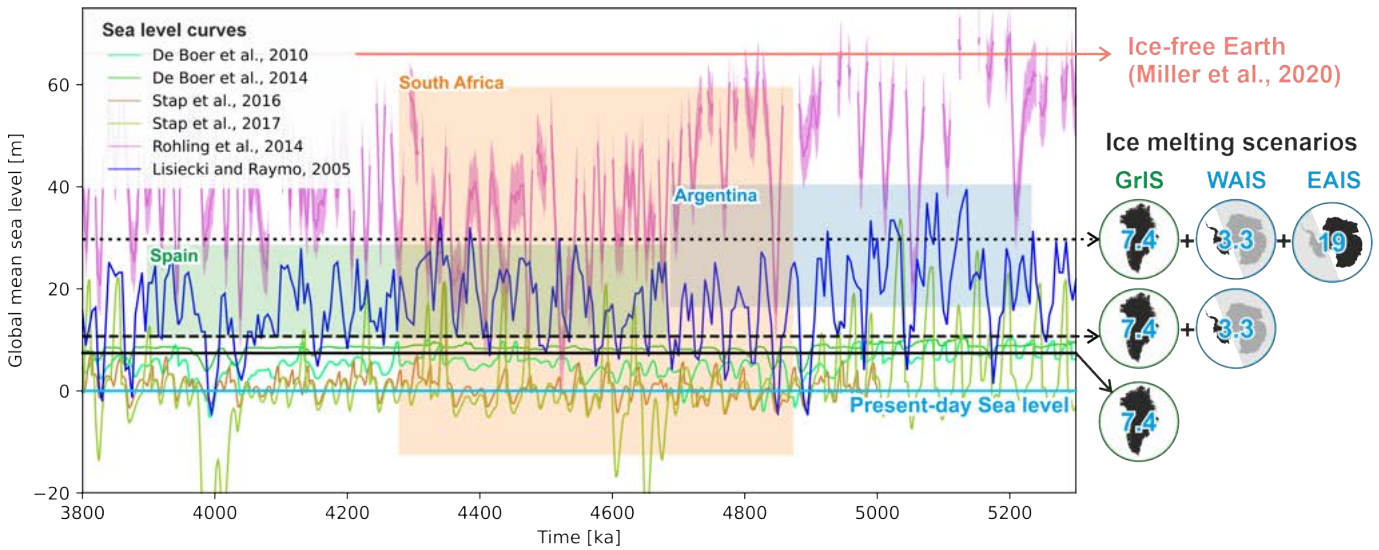


Figure 4: Comparison between sea-level data discussed in this study and global mean sea level derived from ice models<sup>49;50;51;52</sup> and indirect sea level proxies<sup>13;53</sup>. The blue curve shows the GMSL prediction that is used in the GIA model and based on scaling the benthic oxygen isotope record by Lisiecki and Raymo (2005)<sup>53</sup> following the steps described in the methods. Age ranges for observations are  $2\sigma$ , while elevation ranges are  $1\sigma$  for Argentina and South Africa, and 16<sup>th</sup>-84<sup>th</sup> percentiles for Spain. Horizontal black lines and graphics on the right side of the graph show total sea level equivalent for ice-free Greenland (GrIS, solid line<sup>54</sup>), melting of West Antarctic Ice Sheet (WAIS, dashed line<sup>55</sup>) and marine sectors of the East Antarctic Ice Sheet (EAIS, dotted line<sup>56</sup>). The upper red line shows GMSL in an ice-free Earth, estimated to 66m by Miller et al. (2020)<sup>15</sup>.

250 tainties related to GIA, Pleistocene global mean sea level and the  
 251 implicit assumption that uplift rates can be linearly extrapolated  
 252 over these time scales<sup>59</sup>.

253 Despite the uncertainties related to VLMs, there is overlap between  
 254 the calculated global mean sea levels for Camarones ( $28.4 \pm 11.7\text{m}$ ,  $1\sigma$ ) and Coves d'Artá (Spain<sup>9</sup>,  $25.1\text{m}$ , with 16<sup>th</sup>-  
 255 84<sup>th</sup> percentiles of 10.6-28.3m, Figure 3a,b). Correcting the  
 256 proxy record at Cliffs Point (South Africa<sup>10</sup>) with the same GIA  
 257 models used for Camarones (Table 2), results in a paleo RSL  
 258 of  $44.7 \pm 2.7\text{m}$  ( $1\sigma$ ) above present. The DT model predictions  
 259 by Müller et al. (2018)<sup>47</sup>, which were also used for Camarones,  
 260 indicate VLMs in the range of  $4.6 \pm 7.8\text{m/Ma}$  ( $1\sigma$ ). This results  
 261 in an average global mean sea level estimate that aligns with  
 262 those obtained from the other two sites, but bounded by very  
 263 large uncertainties ( $23.4 \pm 35.8\text{m}$ ,  $1\sigma$ ), Figure 3b). As already  
 264 underlined by Hearty et al. (2020)<sup>10</sup>, improving uplift estimates  
 265 for this region is paramount to enable the use of RSL data in  
 266 GMSL calculations.

268 The average global mean sea level calculated from the geological  
 269 facies reported in Argentina (this study), South Africa<sup>10</sup>  
 270 and Spain<sup>9</sup> is well above modern sea level. Compared to published  
 271 global mean sea level estimates that are based on ice sheet  
 272 models and indirect sea-level proxies (Figure 4), it is evident  
 273 that field evidence is most consistent with the highstands  
 274 obtained by scaling the Lisiecki and Raymo (2004)<sup>53</sup> benthic  
 275 oxygen isotope stack (see Methods for details). Our data is also  
 276 consistent with some peaks predicted by the one-dimensional  
 277 ice sheet model of Stap et al. (2017)<sup>52</sup>. Other ice sheet model  
 278 based estimates<sup>49;50;51</sup> significantly under predict the observed  
 279 Early Pliocene sea level records presented here. The almost-  
 280 continuous Gibraltar record<sup>13</sup>, derived from planktic  $\delta^{18}\text{O}$  cou-

281 pled with a hydraulic model, largely over predicts sea level  
 282 observed at both Argentina and Spain suggesting that, when the  
 283 Camarones outcrop was deposited, the Earth was substantially  
 284 ice-free. To align with this record, the three sites in this study  
 285 would have to be characterized by marked subsidence, instead  
 286 of uplift as indicated by almost all dynamic topography models  
 287 we considered. Early Pliocene observations from Argentina only  
 288 overlap with lowstands of the Gibraltar record, which would  
 289 have left regressive imprints. This is at odds with the sedi-  
 290 mentological characteristics of the *Roacut*, which represents a  
 291 transgressive system rather than a regressive one.

292 While GMSL estimates from South Africa<sup>10</sup> are affected by  
 293 large uncertainties, their average value together with the Arg-  
 294 entinian sea-level proxies presented in this study and those  
 295 obtained from Spain<sup>9</sup>, suggest that Early Pliocene GMSL might  
 296 have exceeded 20m above present-day levels. Reaching the average  
 297 GMSL calculated for Camarones (28.4m) would require an ice-free  
 298 Greenland (GrIS, 7.4m sea-level equivalent<sup>54</sup>), significant melting  
 299 of the West Antarctic Ice Sheet (WAIS, 3.3m sea-level equivalent<sup>55</sup>)  
 300 and the almost complete melting of marine sectors of the East  
 301 Antarctic Ice Sheet (EAIS, 19m sea-level equivalent<sup>56</sup>). Reaching  
 302 the lower end calculated for Camarones (16.7m,  $1\sigma$  below the mean)  
 303 would require complete melting of the GrIS and WAIS, and melting  
 304 of about 1/3 of the marine-based sectors of the EAIS. This scenario  
 305 would match almost exactly a complete GrIS melting, and a contribution  
 306 from Antarctica in line with the one modelled by Golledge et al. (2007)<sup>60</sup>.  
 307 These authors calculated that the contribution of Antarctica to  
 308 GMSL during an Early Pliocene (4.23Ma) interglacial was 8.5m,  
 309 sourced primarily from WAIS and the Wilkes subglacial basin of  
 310 EAIS. Reaching the upper end calculated for Camarones (40.1m,  
 311

312  $1\sigma$  above the mean) would require significant contributions of  
 313 not only marine-based but also land-based sectors of the EAIS  
 314 in addition to melting of the GrIS and WAIS. We note that geo-  
 315 logical proxies suggest that a significant melting of land-based  
 316 portions of EAIS was unlikely over the past 8 million years<sup>61</sup>,  
 317 which makes this last scenario less likely.

## 318 CONCLUSIONS

319 The Early Pliocene world was characterized by global annual  
 320 mean temperatures of 2-3°C higher than pre-industrial, and CO<sub>2</sub>  
 321 levels between 280 and 450 ppm<sup>16</sup>. In face of these relatively  
 322 small differences in temperature and CO<sub>2</sub>, the Earth's climate  
 323 was substantially different than today<sup>17</sup>, and ice sheets were  
 324 significantly smaller. Until recently, field evidence to support  
 325 the answer to the question "How high was global mean sea level  
 326 in the Early Pliocene?" was elusive. In this study, we show that  
 327 independent paleo sea-level indicators of similar age on three  
 328 continents result in broadly similar GMSL estimates. While  
 329 affected by large uncertainties, stemming mostly from vertical  
 330 land motion estimates, they indicate that Early Pliocene sea  
 331 level may have exceeded 20m above present-day. This value can  
 332 be attained only with a complete melting of the Greenland ice  
 333 sheet and significant contributions of Antarctica (also including  
 334 marine-based sectors of East Antarctica).

335 The significance of the Early Pliocene and its potential role  
 336 as analog for present-day and near-future warming must be  
 337 taken into account as the world prepares to meet the "Paris  
 338 Agreement"<sup>62</sup> goals and limit global warming below the 1.5°C  
 339 threshold<sup>63</sup>.

## 340 METHODS

341 **Elevation measurements and paleo RSL estimates.** We  
 342 measured elevations with a differential GPS system (Trimble  
 343 ProXRT receiver and Trimble Tornado antenna) equipped to  
 344 receive OmniSTAR HP real-time corrections. As per technical  
 345 specifications by the service provider, these corrections allow to  
 346 measure, in optimal conditions, the elevation of a point with an  
 347 accuracy of 0.1-0.6 m ( $2\sigma$ ), depending on the survey conditions.  
 348 We remark that, while at the *Caprock* outcrop there is a free view  
 349 of the sky, at the *Roadcut* satellite reception is hindered by the  
 350 vertical cliff face. This could explain, in part, the discrepancy  
 351 in the two points collected at this outcrop at relatively short  
 352 distance from each other. Data were originally recorded  
 353 in geographic WGS84 coordinates and in height above the  
 354 ITRF2008 ellipsoid. For each GPS point, we calculated heights  
 355 above Mean Sea Level (orthometric height) subtracting from  
 356 the measured ITRF2008 ellipsoid height the GEOIDEAR16  
 357 geoid height<sup>41</sup>. These geoidal elevations are the best available  
 358 approximation of mean sea level in this area. GEOIDEAR16  
 359 was estimated to have an overall accuracy of 10 cm  
 360 ([https://www.ign.gob.ar/NuestrasActividades/Geodesia/Geoide-  
 361 Ar16](https://www.ign.gob.ar/NuestrasActividades/Geodesia/Geoide-Ar16)). The location and elevations of Unit **Cp** at *Roadcut* and  
 362 *Caprock* are reported in Table 1.

363 From these elevations, we calculate that the average elevation  
 364 ( $\mu E$ ) is 36.2m. To calculate the elevation error ( $\sigma E$ ), we use the  
 365 following formula:

$$\sigma E = \sqrt{\frac{\sum_1^N (\sigma E_p^2 \cdot (p-1)) + p \cdot (\mu E - \mu E_p)}{N-1}} \quad (1)$$

366 Where N is the total number of filtered positions measured by  
 367 the GPS during the survey (439, sum of "Number of filtered  
 368 positions" in Table 1),  $\sigma E_p$  is the elevation error for each single  
 369 point,  $\mu E_p$  is the Height above geoid of each single point and  
 370  $\mu E$  is the average elevation (36.2m) (Table 1). On average, we  
 371 calculate that the elevation of Unit **Cp** is  $36.2 \pm 0.9\text{m}$  ( $1\sigma$ ).

372 The Unit **Cp** at the *Roadcut* and *Caprock* sites has been inter-  
 373 preted as forming in the foreshore zone, i.e., in the intertidal  
 374 zone. This means that its indicative meaning<sup>64</sup> spans from  
 375 Mean Lower Low Water (MLLW) to Mean Higher High Wa-  
 376 ter (MHHW). Based on predicted tidal data for the harbor of  
 377 Camarones, Bini et al. (2018)<sup>37</sup> report that the maximum tidal  
 378 range (MHHW to MLLW) in Camarones is 5m. We use this  
 379 value (5m) as the indicative range (IR) for a foreshore deposit in  
 380 our area, and the midpoint between MHHW and MLLW (0m)  
 381 as reference water level (RWL). Then, using the formulas de-  
 382 scribed in Rovere et al. (2016)<sup>1</sup>, we calculate paleo RSL and its  
 383 associated uncertainty as follows: 384

$$RSL = \mu E - RWL \quad (2)$$

$$\sigma RSL = \sqrt{\sigma E^2 + \left(\frac{IR}{2}\right)^2} \quad (3)$$

385 Using the equations above, we calculate that paleo RSL associ-  
 386 ated with Unit **Cp** is  $36.2 \pm 2.7\text{m}$ . We highlight that this value  
 387 does not take into account the possibility that, 5 Ma ago, tidal  
 388 ranges were different than present-day ones, due to different  
 389 shelf bathymetry under higher sea levels<sup>65</sup>.

390 To calculate global mean sea level (GMSL) and associated un-  
 391 certainties, we used the following formulas:

$$GMSL = RSL - \mu GIA - \mu VLM \quad (4)$$

392 Where  $\mu GIA$  is the average of the GIA models (Table 2) and  
 393  $\mu VLM$  is calculated as the product of mean dynamic topography  
 394 rate (Table 3) multiplied by the average age of the deposit. 395

$$\sigma GMSL = \sqrt{\sigma RSL^2 + \sigma GIA^2 + \sigma VLM^2} \quad (5)$$

396 Where  $\sigma GIA$  is the standard deviation of GIA models shown in  
 397 Table 2 and  $\sigma VLM$  is calculated as follows: 398

$$\sigma VLM = |VLM| \cdot \sqrt{\left(\frac{\sigma Age}{\mu Age}\right)^2 + \left(\frac{\sigma Rate}{\mu Rate}\right)^2} \quad (6)$$

399 Where  $\mu Age$  and  $\sigma Age$  are the average and  $1\sigma$  age of the deposit,  
 400 and  $\mu Rate$  and  $\sigma Rate$  are the average and  $1\sigma$  rates derived from  
 401 published dynamic topography models (Table 3). 402

Table 1: GPS position and elevation of Unit **Cp** measured at the *Roadcut* and *Caprock* sites. Lat/Lon are in WGS84 coordinates, Ellipsoid heights are referred to the ITRF08 ellipsoid, geoid heights to the GEOIDEAR16 geoid model.

Longitude (decimal degrees E)	Latitude (decimal degrees N)	Ellipsoid Height (m)	Height above geoid ( $\mu E_p$ ) (m)	Elevation error ( $\sigma E$ ) (m)	Number of filtered positions (p)
<b>Roadcut</b>					
-65.727604	-44.790083	49.67	36.8	0.06	27
-65.727619	-44.790069	47.68	34.8	0.28	134
<b>Caprock</b>					
-65.728221	-44.799297	49.40	36.5	0.17	249
-65.728221	-44.799298	49.64	36.8	0.12	29
Average			<b>36.2</b>		

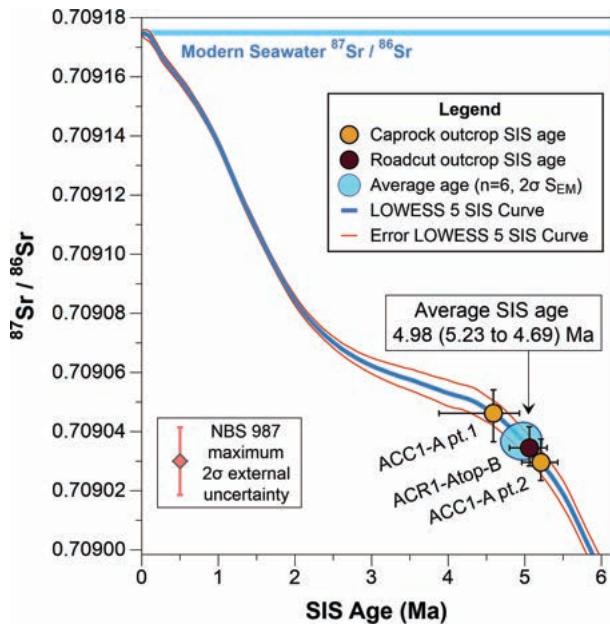


Figure 5: Sr isotope stratigraphy relative ages of oyster shells plotted on the SIS curve (LOWESS version 5)<sup>66</sup>. Orange points are from two separate portions of a shell from the *Caprock*, while maroon point is of a shell from unit **Cp** in the *Roadcut*. The average SIS age based on these samples is shown as a blue ellipse. Only inner leaches on the best-preserved specimens are shown. For the full dataset, see Supplementary Note 3 annexed to this paper. Modern seawater  $^{87}\text{Sr}/^{86}\text{Sr}$  values shown in light blue line. Maximum  $2\sigma$  external uncertainty for the Sr isotope external standard NBS 987 is shown as red point for comparison (see Methods for details).

399 **Strontium Isotope Stratigraphy ages.** To attribute an age  
 400 to Unit **Cp**, we used the Strontium Isotope Stratigraphy (SIS)  
 401 curve published by McArthur et al. (2012)<sup>66</sup> (LOWESS version  
 402 5). Sr isotope ratios from carbonates are susceptible to post-  
 403 depositional alteration, therefore, any significant reworking of  
 404 Sr isotopes needs to be detected and discarded. Information on  
 405 shell preservation was determined using  $^{87}\text{Sr}/^{86}\text{Sr}$  measurements  
 406 on sequentially leached shell material (assuming smaller Sr iso-  
 407 tope variations between leaches implies better preservation<sup>67,68</sup>)  
 408 alongside standard screening techniques<sup>36,69</sup> and elemental anal-

409 ysis<sup>70,71</sup>). A preservation index between "1" (unaltered) and  
 410 "3" (highly altered) was established for each sample based on  
 411 these criteria (Supplementary Note 3, Supplementary Figures  
 412 3-7, Supplementary Table 3-4) with samples scoring above "2.0"  
 413 excluded from results. The same screening criteria have recently  
 414 been used by Hearty et al. (2020)<sup>10</sup> and are discussed in Sand-  
 415 strom et al. (2020)<sup>11</sup>. The latter also gives an overview of  
 416 the limits and implications of SIS analyses for Plio-Pleistocene  
 417 marine samples.

418 We selected Ostreidae species for SIS chronological constraints,  
 419 primarily because these shells precipitate original calcite min-  
 420 eral phases, making them more robust to diagenesis than arag-  
 421 onitic shells. Sample screening and chemical processing was  
 422 carried out at Lamont Doherty Earth Observatory (LDEO), and  
 423 all  $^{87}\text{Sr}/^{86}\text{Sr}$  measurements were made using Thermal Ion Mass  
 424 Spectrometry (TIMS) on an IsotopX Phoenix at SUNY Stony-  
 425 brook University (SBU) or a Finnigan Triton Plus at Lamont  
 426 Doherty Earth Observatory (LDEO).

427 We measured three oyster shells, one from the *Caprock* and two  
 428 from the *Roadcut* unit. The *Caprock* oyster (ACC1-A) was sam-  
 429 pled in three different locations, with inner leaches measured  
 430 on two of those splits, returning SIS ages of 4.59Ma (3.88 to  
 431 4.93Ma) and 5.21Ma (4.96 to 5.44Ma) (Figure 5). The third  
 432 sampling location was only measured for full dissolution, with  
 433 an average SIS age of 4.65Ma (4.42 to 4.83Ma), but provided  
 434 confidence in the shell Sr isotope heterogeneity and validated  
 435 analytical uncertainties. The preservation index score for the  
 436 caprock oyster(pt.1) was 1.92. The two shells measured from the  
 437 *Roadcut* (ACR1-Atop-B and ACR1-Ctop-C) had inner leach SIS  
 438 ages of 5.06Ma (4.80 to 5.28Ma), and 6.35Ma (6.19 to 6.53Ma),  
 439 respectively. Additional diagenesis screening techniques on  
 440 these shells included elemental analysis (Supplementary Note  
 441 3), and variation of  $^{87}\text{Sr}/^{86}\text{Sr}$  within the leach set of each sam-  
 442 ple. The results of sample variation compared to the inner leach  
 443  $^{87}\text{Sr}/^{86}\text{Sr}$  are shown in the Supplementary Note 3, with low Sr  
 444 isotope variation indicative of better preservation. Samples with  
 445 low variation tend to exhibit more radiogenic  $^{87}\text{Sr}/^{86}\text{Sr}$  values.  
 446 Sample ACR1-Atop-B had a preservation index of 1.56, while  
 447 ACR1-Ctop-C had a score of 2.33 (Supplementary Table 3).  
 448 Based on these screening criteria, we exclude sample ACR1-  
 449 Ctop-C, which appeared to have been altered by low  $^{87}\text{Sr}/^{86}\text{Sr}$   
 450 fluids (possibly of through leaching of surrounding volcanic  
 451 material from the Complejo Marifil<sup>39</sup>). The remaining inner  
 452 leaches that passed screening were averaged by filament to ob-



tain an age of  $4.98 \pm 0.245/-0.295$  Ma ( $n=6$ ,  $2\sigma$   $S_{EM}$ ). In the text, this age is reported as a  $2\sigma$  range, i.e., 4.69-5.23 Ma.

**Glacial Isostatic Adjustment.** To account for changes in vertical displacement and gravity field caused by GIA we use a gravitationally self-consistent sea level model, that accounts for the migration of shorelines and feedback of Earth’s rotation axis<sup>72</sup>. We compute both the contribution to GIA from the amount of residual deformation caused by the most recent Pleistocene glacial cycles and from ice age cycles during the Pliocene.

For the first contribution we use the results from Raymo et al. (2011)<sup>2</sup>, who calculated the residual deformation associated with the ice model ICE-5G<sup>73</sup>. This ice history is paired with a suite of 36 different earth models with varying lithospheric thickness (48km, 71km, and 96km), upper and lower mantle viscosities ( $3 \times 10^{20}$  and  $5 \times 10^{20}$  Pa s for the upper mantle, and  $3 \times 10^{21}$  -  $30 \times 10^{21}$  for the lower mantle) to calculate a mean and standard deviation in residual deformation (Figure 6).

For the second contribution we follow the approach described in Dumitru et al. (2019)<sup>9</sup> by estimating ice mass variability based on the benthic stack<sup>53</sup>. Following Miller et al. (2012)<sup>74</sup> we prescribe that 75% of the benthic  $\delta^{18}O$  variability is due to ice volume changes (the rest being due to temperature) and a further scaling of  $0.11\text{‰}/10\text{m}$  to convert  $\delta^{18}O_{seawater}$  into ice volume changes. These conversions are highly uncertain<sup>75:76</sup>, which highlights the need to obtain local sea level based ice volume estimates. Nonetheless, this scaling was used because it yielded comparable ice volume estimates to the results of Dumitru et al. (2019)<sup>9</sup>. To construct an ice history following this ice volume curve we only assume changes in Antarctic ice volume given evidence that continent wide expansion of northern hemisphere ice sheets did only start around 3.3 Ma<sup>77</sup>. However, we acknowledge that an earlier intermittent Greenland ice sheet might have existed<sup>78</sup>. We compute glacial isostatic adjustment using this ice history and the same suite of 36 different earth models described above. We extract local predictions of relative sea level for Argentina, Mallorca, and South Africa. To calculate global mean sea level changes we integrate the amount of water in the ocean basins as a function of time. We next calculate how this quantity has changed relative to the initial state and divide it by the oceanic area calculated at each time.

Note that this setup to calculate the GIA correction deviates slightly from the one described in Dumitru et al. (2019)<sup>9</sup> in three small ways, (1) we only consider one GMSL history for the Pliocene rather than a range of histories, (2) we only consider variability in southern hemisphere ice sheets and (3) we calculated GMSL as described above rather than as changes in grounded ice volume.

The GIA corrections from both processes are combined. In a last step we consider the age range for each sea level indicator and average the GIA correction during warm periods, which we define as times that had higher than average sea level over this time period<sup>9</sup>. The mean and standard deviation that is obtained is shown in Table 2. We also show the GIA correction calculated by Dumitru et al. (2019)<sup>9</sup> and note that the difference in mean GIA estimates stems mostly from our different definition of global mean sea level. For the analysis in the main text we use

the GIA correction described in Dumitru et al. (2019)<sup>9</sup> for the datapoint from Mallorca and not the one recalculated here.

Table 2: GIA correction for Pliocene sea level markers at the three locations discussed in the text. For comparison, we also report the results for Mallorca used in Dumitru et al.<sup>9</sup>.

Location	Longitude	Latitude	$\mu GIA$ (m)	$\sigma GIA$ (m)
Argentina	65.73° E	44.79° S	-14.6	3.2
South Africa	18.12° W	31.59° S	-9.6	1.6
Mallorca	3.45° W	39.66° N	2.9	2.2
Mallorca <sup>9</sup>	3.45° W	39.66° N	1.3	3.1

**Vertical Land Motions.** VLMs were extracted from published Dynamic Topography models<sup>46:47</sup>. The values extracted are reported in Table 3. Flament et al. (2015)<sup>46</sup> focus on the surface expression of subduction dynamics in South America. Their results are based on forward advection modeling with different tectonic surface boundary conditions. The different cases are based on different timings of slab flattening. Müller et al. (2018)<sup>47</sup> have a global focus and combine back advection (initialized with a seismic tomography model) and forward advection with tectonic surface boundary conditions. Their different models are based on different surface plate reconstructions and different viscosity profiles.

Table 3: Amount of Vertical Land Motion (VLM) at Camarones from two different studies. Predictions are given at the time step closest to the sea level indicator age, which is denoted as ‘Timing’. Rates are calculated based on this age and the predicted VLM and linearly interpolated to the age of the indicator.

Reference	Model	VLM (m)	Timing (Ma)	Rate (m/Ma)
Müller et al. (2018) <sup>47</sup>	M1	4.6	10	0.46
	M2	66.2	10	6.62
	M3	45.0	10	4.50
	M4	58.0	10	5.80
	M5	45.4	10	4.54
	M6	21.8	10	2.18
	M7	25.5	10	2.55
Flament et al. (2015) <sup>46</sup>	Case 1	35.7	5	7.14
	Case 2	37.6	5	7.52
	Case 3	22.9	5	4.58
	Case 4	18.6	5	3.73

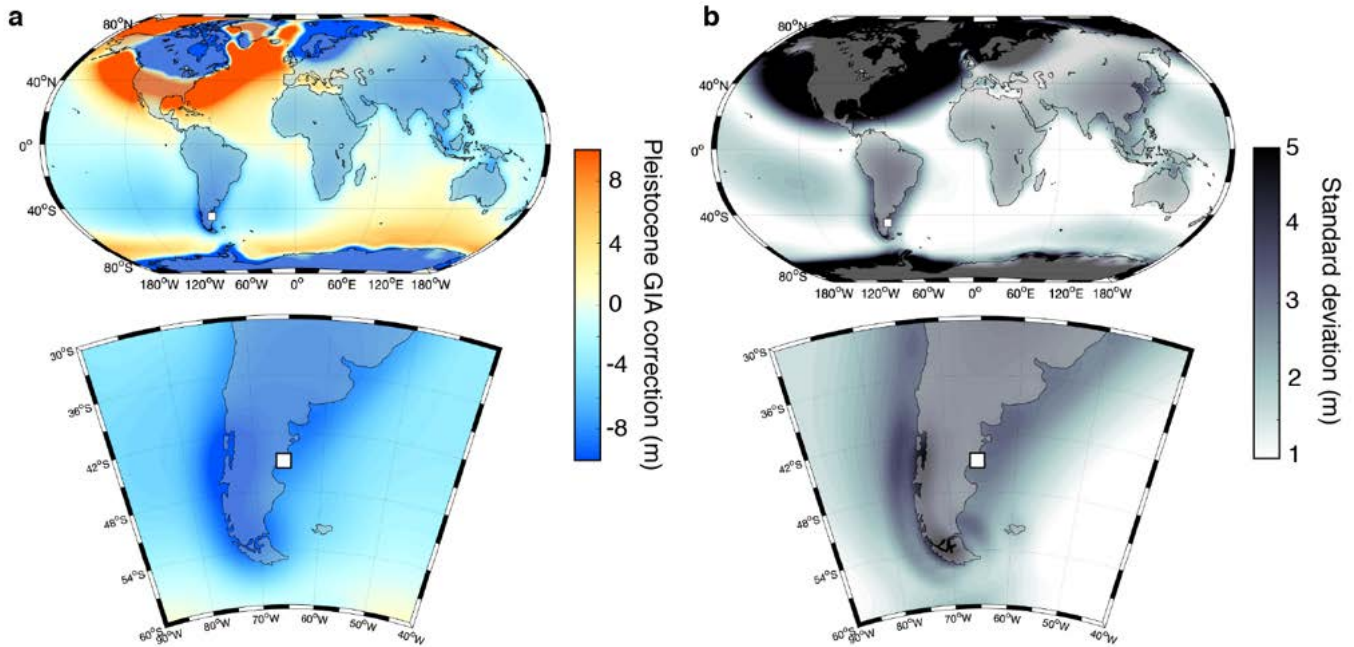


Figure 6: GIA contribution due to ongoing adjustment. The maps show the GIA contribution caused by the incomplete present-day adjustment to the late Pleistocene ice and ocean loading cycles. **a)** Model simulation using a viscosity structure of  $5 \times 10^{20}$  Pa s viscosity in the upper mantle,  $5 \times 10^{21}$  Pa s viscosity in the lower mantle, and an elastic lithospheric thickness of 96 km. **b)** Standard deviation of model predictions obtained using 36 different radial viscosity profiles, including varying the lithospheric thickness. The square in all insets marks the position of Camarones.

524 DATA AVAILABILITY

525 Spreadsheets containing GPS data, GMSL calculations, and  
 526 details on shell preservation and ages are available from  
 527 <https://doi.org/10.5281/zenodo.3929150><sup>40</sup> (CC-BY 4.0 license).  
 528 The GEOIDEAR16 geoid model was created by the Insti-  
 529 tuto Geográfico Nacional (Ministerio de Defensa, Argentina)  
 530 and it was retrieved from the International Service for  
 531 the Geoid <http://www.isgeoid.polimi.it/>. Plate boundaries  
 532 in Figure 1 and Figure 3 were downloaded from GitHub:  
 533 <https://github.com/fraxen/tectonicplates/> (ODC-By license), and  
 534 are derived from data by Peter Bird<sup>48</sup>, Hugo Ahlenius and  
 535 Nordpil. The background shoreline maps in Figure 3A and  
 536 Figure 6 were retrieved from NOAA-NCEI (Global Self-  
 537 consistent Hierarchical High-resolution Shoreline, GSHHS<sup>79</sup>).  
 538 Equation (1) was derived from a StackExchange discus-  
 539 sion ([https://stats.stackexchange.com/questions/25848/how-to-](https://stats.stackexchange.com/questions/25848/how-to-sum-a-standard-deviation)  
 540 [sum-a-standard-deviation](https://stats.stackexchange.com/questions/25848/how-to-sum-a-standard-deviation)). Samples described in this study  
 541 were registered in the System for Earth Sample Registration  
 542 <https://www.geosamples.org/>, and assigned an International Geo-  
 543 Sample number (IGSN). Dynamic topography model outputs  
 544 were obtained from the Gplates portal (<http://portal.gplates.org/>).

545 CODE AVAILABILITY

546 The python scripts used to produce panels b and c of  
 547 Figure 3 and the main panel of Figure 4 are available  
 548 from <https://doi.org/10.5281/zenodo.3689426><sup>80</sup> (MIT license).  
 549 The computer code used to do the sea-level (GIA) cal-

550 culation, written in MATLAB, is available on GitHub  
 551 (<https://github.com/jaustermann/SLcode>).

552 ACKNOWLEDGMENTS

553 This research was among the primary objectives of the  
 554 PLIOMAX grant, NSF OCE-1202632 (PI MER and co-PI PJH).  
 555 AR acknowledges the Institutional Strategy of the University  
 556 of Bremen, German Excellence Initiative (ABPZuK-03/2014).  
 557 MER and JA acknowledge the additional support of the G. Unger  
 558 Vetlesen Foundation. MA acknowledges the following projects:  
 559 Agencia Nacional de Promoción Científica y Tecnológica (PICT  
 560 2006-468, PICT 2013-1298), CONICET (PIP 0080, 0372 and  
 561 0729), and Universidad Nacional de La Plata (PI N11/587 and  
 562 N11/726). The authors acknowledge PALSEA for useful dis-  
 563 cussions during annual meetings. PALSEA is a working group  
 564 of the International Union for Quaternary Sciences (INQUA)  
 565 and Past Global Changes (PAGES), which in turn received sup-  
 566 port from the Swiss Academy of Sciences and the Chinese  
 567 Academy of Sciences. We acknowledge Deirdre Ryan and Evan  
 568 Gowan for useful discussions in the field, and Karla Rubio San-  
 569 doval Zurisadai for comments on the final draft of the MS. The  
 570 background maps in Figure 1 of this article were created using  
 571 ArcGIS<sup>®</sup> software by Esri. ArcGIS<sup>®</sup> and ArcMap<sup>™</sup> are the  
 572 intellectual property of Esri and are used herein under license.  
 573 Copyright<sup>©</sup> Esri. All rights reserved. For more information  
 574 about Esri<sup>®</sup> software, please visit [www.esri.com](http://www.esri.com).

## 575 AUTHOR CONTRIBUTIONS

576 AR, MP and SR wrote the MS and supplementary materials,  
 577 including figures. SR elaborated the stratigraphic description  
 578 of the *Roadcut* outcrop. MA provided expertise on the faunal  
 579 composition of the *Roadcut* and *Caprock* outcrops. MRS per-  
 580 formed SIS dating and contributed text on SIS methods and  
 581 results. JA produced GIA estimates, advised on DT and GMSL  
 582 calculations, and contributed to the writing of the paper. PJH  
 583 provided expertise on stratigraphic and geological interpretation  
 584 on the Camarones outcrops. All authors (except JA) participated  
 585 in different phases of the field expeditions to Camarones. IC  
 586 identified the *Caprock* site in the field. MER provided expertise  
 587 on the paleoclimatic implications of the study. All authors re-  
 588 visited the main text and Supplementary Information, and agree  
 589 with its contents.

## 590 COMPETING INTERESTS

591 The authors declare no competing interests

## 592 REFERENCES

- 593 [1] Rovere, A. *et al.* The analysis of last interglacial (mis 5e)  
 594 relative sea-level indicators: Reconstructing sea-level in  
 595 a warmer world. *Earth-Science Reviews* **159**, 404–427  
 596 (2016).
- 597 [2] Raymo, M. E., Mitrovica, J. X., O’Leary, M. J., DeConto,  
 598 R. M. & Hearty, P. J. Departures from eustasy in pliocene  
 599 sea-level records. *Nature Geoscience* **4**, 328–332 (2011).
- 600 [3] Austermann, J., Mitrovica, J. X., Huybers, P. & Rovere,  
 601 A. Detection of a dynamic topography signal in last inter-  
 602 glacial sea-level records. *Science Advances* **3**, e1700457  
 603 (2017).
- 604 [4] Dutton, A. *et al.* Sea-level rise due to polar ice-sheet  
 605 mass loss during past warm periods. *science* **349**, aaa4019  
 606 (2015).
- 607 [5] DeConto, R. M. & Pollard, D. Contribution of antarctica to  
 608 past and future sea-level rise. *Nature* **531**, 591–597 (2016).
- 609 [6] Khan, N. S. *et al.* Inception of a global atlas of sea lev-  
 610 els since the last glacial maximum. *Quaternary Science*  
 611 *Reviews* **220**, 359–371 (2019).
- 612 [7] Pedoja, K. *et al.* Coastal staircase sequences reflecting sea-  
 613 level oscillations and tectonic uplift during the quaternary  
 614 and neogene. *Earth-Science Reviews* **132**, 13–38 (2014).
- 615 [8] Rovere, A. *et al.* The mid-pliocene sea-level conundrum:  
 616 Glacial isostasy, eustasy and dynamic topography. *Earth*  
 617 *and Planetary Science Letters* **387**, 27–33 (2014).
- 618 [9] Dumitru, O. A. *et al.* Constraints on global mean sea level  
 619 during pliocene warmth. *Nature* **574**, 233–236 (2019).
- 620 [10] Hearty, P. J. *et al.* Pliocene-pleistocene stratigraphy  
 621 and sea-level estimates, republic of south africa with  
 622 implications for a 400 ppmv co2 world. *Paleoceanography*  
 623 *and Paleoclimatology* **35**, e2019PA003835 (2020). URL  
 624 [https://agupubs.onlinelibrary.wiley.com/](https://agupubs.onlinelibrary.wiley.com/doi/abs/10.1029/2019PA003835)  
 625 [doi/abs/10.1029/2019PA003835](https://doi/abs/10.1029/2019PA003835). E2019PA003835  
 626 2019PA003835, [https://agupubs.onlinelibrary.](https://agupubs.onlinelibrary.wiley.com/doi/pdf/10.1029/2019PA003835)  
 627 [wiley.com/doi/pdf/10.1029/2019PA003835](https://doi/pdf/10.1029/2019PA003835).
- [11] Sandstrom, M. R. *et al.* Age constraints on surface  
 deformation recorded by fossil shorelines at Cape  
 Range, Western Australia. *GSA Bulletin* (2020). URL  
<https://doi.org/10.1130/B35564.1>. [https://pubs.geoscienceworld.org/gsabulletin/](https://pubs.geoscienceworld.org/gsabulletin/article-pdf/doi/10.1130/B35564.1/5135376/b35564.pdf)  
[article-pdf/doi/10.1130/B35564.1/5135376/](https://pubs.geoscienceworld.org/gsabulletin/article-pdf/doi/10.1130/B35564.1/5135376/b35564.pdf)  
[b35564.pdf](https://pubs.geoscienceworld.org/gsabulletin/article-pdf/doi/10.1130/B35564.1/5135376/b35564.pdf).
- [12] United States Geological Survey. Shuttle radar topography  
 mission (SRTM) 1 arc-second global. version 3.0 (2015).
- [13] Rohling, E. *et al.* Sea-level and deep-sea-temperature  
 variability over the past 5.3 million years. *Nature* **508**,  
 477–482 (2014).
- [14] Raymo, M. E., Kozdon, R., Evans, D., Lisiecki, L. & Ford,  
 H. L. The accuracy of mid-pliocene  $\delta 18\text{o}$ -based ice volume  
 and sea level reconstructions. *Earth-Science Reviews* **177**,  
 291–302 (2018).
- [15] Miller, K. G. *et al.* Cenozoic sea-level and cryospheric  
 evolution from deep-sea geochemical and continental  
 margin records. *Science Advances* **6** (2020). URL  
[https://advances.sciencemag.org/content/6/](https://advances.sciencemag.org/content/6/20/eaaz1346)  
[20/eaaz1346](https://advances.sciencemag.org/content/6/20/eaaz1346). [https://advances.sciencemag.org/](https://advances.sciencemag.org/content/6/20/eaaz1346.full.pdf)  
[content/6/20/eaaz1346.full.pdf](https://advances.sciencemag.org/content/6/20/eaaz1346.full.pdf).
- [16] Haywood, A. M. *et al.* Are there pre-quaternary geological  
 analogues for a future greenhouse warming? *Philosophical*  
*Transactions of the Royal Society A: Mathematical,*  
*Physical and Engineering Sciences* **369**, 933–956 (2011).
- [17] Fedorov, A. *et al.* Patterns and mechanisms of early  
 pliocene warmth. *Nature* **496**, 43–49 (2013).
- [18] Lunt, D. J. *et al.* Earth system sensitivity inferred from  
 pliocene modelling and data. *Nature Geoscience* **3**, 60–64  
 (2010).
- [19] Grant, G. *et al.* The amplitude and origin of sea-level  
 variability during the pliocene epoch. *Nature* **574**, 237–  
 241 (2019).
- [20] Solgaard, A. M., Reeh, N., Japsen, P. & Nielsen, T.  
 Snapshots of the greenland ice sheet configuration in the  
 pliocene to early pleistocene. *Journal of Glaciology* **57**,  
 871–880 (2011).
- [21] Naish, T. *et al.* Obliquity-paced pliocene west antarctic ice  
 sheet oscillations. *Nature* **458**, 322–328 (2009).
- [22] Pollard, D. & DeConto, R. M. Modelling west antarctic  
 ice sheet growth and collapse through the past five million  
 years. *Nature* **458**, 329–332 (2009).
- [23] Cook, C. P. *et al.* Dynamic behaviour of the east antarctic  
 ice sheet during pliocene warmth. *Nature Geoscience* **6**,  
 765–769 (2013).
- [24] Dolan, A. M. *et al.* Sensitivity of pliocene ice sheets  
 to orbital forcing. *Palaeogeography, Palaeoclimatology,*  
*Palaeoecology* **309**, 98–110 (2011).
- [25] Thomas, C., Livermore, R. & Pollitz, F. Motion of the  
 scotia sea plates. *Geophysical Journal International* **155**,  
 789–804 (2003).
- [26] Rabassa, J. Late cenozoic glaciations in patagonia and  
 tierra del fuego. *Developments in quaternary sciences* **11**,  
 151–204 (2008).

- 683 [27] Guillaume, B., Martinod, J., Husson, L., Rod- 740  
684 daz, M. & Riquelme, R. Neogene uplift of cen- 741  
685 tral eastern patagonia: Dynamic response to ac- 742  
686 tive spreading ridge subduction? *Tectonics* **28** 743  
687 (2009). URL [https://agupubs.onlinelibrary.](https://agupubs.onlinelibrary.wiley.com/doi/abs/10.1029/2008TC002324)  
688 [wiley.com/doi/abs/10.1029/2008TC002324.](https://agupubs.onlinelibrary.wiley.com/doi/pdf/10.1029/2008TC002324)  
689 [https://agupubs.onlinelibrary.wiley.com/doi/](https://agupubs.onlinelibrary.wiley.com/doi/pdf/10.1029/2008TC002324)  
690 [pdf/10.1029/2008TC002324.](https://agupubs.onlinelibrary.wiley.com/doi/pdf/10.1029/2008TC002324)
- 691 [28] Ton-That, T., Singer, B., Mörner, N.-A. & Rabassa, J. Dat- 744  
692 ación de lavas basálticas por 40ar/39ar y geología glacial 745  
693 de la región del lago buenos aires, provincia de santa cruz, 746  
694 argentina. *Revista de la Asociación Geológica Argentina* 747  
695 **54**, 333–352 (1999). 748  
696 [29] Darwin, C. *Geological observations on South America: 749  
697 Being the third part of the geology of the voyage of the 750  
698 Beagle, under the command of Capt. Fitzroy, RN during 751  
699 the years 1832 to 1836* (Smith, Elder and Company, 65, 752  
700 Cornhill., 1846). 753
- 701 [30] Schellmann, G. & Radtke, U. Coastal terraces and 754  
702 holocene sea-level changes along the patagonian atlantic 755  
703 coast. *Journal of Coastal Research* 983–996 (2003). 756
- 704 [31] Zanchetta, G. *et al.* Middle-to late-holocene relative sea- 757  
705 level changes at puerto deseado (patagonia, argentina). *The 758  
706 Holocene* **24**, 307–317 (2014). 759
- 707 [32] Pappalardo, M. *et al.* Coastal landscape evolution and 760  
708 sea-level change: A case study from central patagonia 761  
709 (argentina). *Zeitschrift für Geomorphologie* **59**, 145–172 762  
710 (2015). 763
- 711 [33] Rostami, K., Peltier, W. & Mangini, A. Quaternary marine 764  
712 terraces, sea-level changes and uplift history of patagonia, 765  
713 argentina: comparisons with predictions of the ice-4g 766  
714 (vm2) model of the global process of glacial isostatic ad- 767  
715 justment. *Quaternary Science Reviews* **19**, 1495–1525 768  
716 (2000). 769
- 717 [34] Schellmann, G. & Radtke, U. ESR dating stratigraphically 770  
718 well-constrained marine terraces along the patagonian at- 771  
719 lantic coast (argentina). *Quaternary International* **68**, 261– 772  
720 273 (2000). 773
- 721 [35] Rutter, N. *et al.* Correlation and dating of quaternary 774  
722 littoral zones along the patagonian coast, argentina. *Qua- 775  
723 ternary Science Reviews* **8**, 213–234 (1989). 776
- 724 [36] Del Río, C., Griffin, M., McArthur, J., Martínez, S. & 777  
725 Thirlwall, M. Evidence for early pliocene and late miocene 778  
726 transgressions in southern patagonia (argentina): 87sr/86sr 779  
727 ages of the pectinid "chlamys" actinodes (sowerby). *Jour- 780  
728 nal of South American Earth Sciences* **47** (2013). 781
- 729 [37] Bini, M. *et al.* Mid-holocene relative sea-level changes 782  
730 along atlantic patagonia: new data from camarones, chubut, 783  
731 argentina. *The Holocene* **28**, 56–64 (2018). 784
- 732 [38] Feruglio, E. *Descripción geológica de la Patagonia*, vol. 1 785  
733 (Impr. y Casa Editora "Coni", 1949). 786
- 734 [39] Lema, H. A. *et al.* *Hoja Geológica 4566-II y IV Camarones* 787  
735 (Servicio Geológico Minero Argentino. Instituto de Ge- 788  
736 ología y Recursos Minerales, 2001). 789
- 737 [40] Rovere, A. *et al.* Survey data, models and dated samples of 790  
738 the pliocene shorelines of camarones, argentina (ver 1.1). 791  
739 (2020). 792
- [41] Piñón, D., Zhang, K., Wu, S. & Cimbaro, S. A new argen- 793  
tinean gravimetric geoid model: Geoidear. In *International 794  
Symposium on Earth and Environmental Sciences for Fu- 795  
ture Generations*, 53–62 (Springer, 2017). 796
- [42] Braun, J. The many surface expressions of mantle dynam- 797  
ics. *Nature Geoscience* **3**, 825–833 (2010). 798
- [43] Moucha, R. *et al.* Dynamic topography and long-term 799  
sea-level variations: There is no such thing as a stable 800  
continental platform. *Earth and Planetary Science Letters* 801  
**271**, 101–108 (2008). 802
- [44] Moucha, R. & Ruetenik, G. A. Interplay between dynamic 803  
topography and flexure along the us atlantic passive margin: 804  
Insights from landscape evolution modeling. *Global and 805  
Planetary Change* **149**, 72–78 (2017). 806
- [45] Ferrier, K. L., Austermann, J., Mitrovica, J. X. & Pico, T. 807  
Incorporating sediment compaction into a gravitationally 808  
self-consistent model for ice age sea-level change. *Geo- 809  
physical Journal International* **211**, 663–672 (2017). 810
- [46] Flament, N., Gurnis, M., Müller, R. D., Bower, D. J. & 811  
Husson, L. Influence of subduction history on south amer- 812  
ican topography. *Earth and Planetary Science Letters* **430**, 813  
9–18 (2015). 814
- [47] Müller, R. D., Hassan, R., Gurnis, M., Flament, N. & 815  
Williams, S. E. Dynamic topography of passive conti- 816  
nental margins and their hinterlands since the Cretaceous. 817  
*Gondwana Research* **53**, 225–251 (2018). 818
- [48] Bird, P. An updated digital model of plate boundaries. 819  
*Geochemistry, Geophysics, Geosystems* **4** (2003). 820
- [49] De Boer, B., Van de Wal, R., Bintanja, R., Lourens, L. & 821  
Tuenter, E. Cenozoic global ice-volume and temperature 822  
simulations with 1-d ice-sheet models forced by benthic  $\delta$  823  
18 o records. *Annals of glaciology* **51**, 23–33 (2010). 824
- [50] De Boer, B., Lourens, L. J. & Van De Wal, R. S. Persistent 825  
400,000-year variability of antarctic ice volume and the 826  
carbon cycle is revealed throughout the plio-pleistocene. 827  
*Nature Communications* **5**, 2999 (2014). 828
- [51] Stap, L. B. *et al.* CO<sub>2</sub> over the past 5 million years: Con- 829  
tinuous simulation and new  $\delta$ 11b-based proxy data. *Earth 830  
and Planetary Science Letters* **439**, 1–10 (2016). 831
- [52] Stap, L. B., Van De Wal, R. S., De Boer, B., Bintanja, 832  
R. & Lourens, L. J. The influence of ice sheets on tem- 833  
perature during the past 38 million years inferred from a 834  
one-dimensional ice sheet-climate model. *Climate of the 835  
Past* **13**, 1243–1257 (2017). 836
- [53] Lisiecki, L. E. & Raymo, M. E. A pliocene-pleistocene 837  
stack of 57 globally distributed benthic  $\delta$ 18o records. *Pa- 838  
leocanography* **20** (2005). 839
- [54] Morlighem, M. *et al.* Bedmachine v3: Complete bed top- 840  
ography and ocean bathymetry mapping of greenland 841  
from multibeam echo sounding combined with mass con- 842  
servation. *Geophysical research letters* **44**, 11–051 (2017). 843
- [55] Bamber, J. L., Riva, R. E., Vermeersen, B. L. & LeBrocq, 844  
A. M. Reassessment of the potential sea-level rise from 845  
a collapse of the west antarctic ice sheet. *science* **324**, 846  
901–903 (2009). 847

- 795 [56] Fretwell, P. *et al.* Bedmap2: improved ice bed, surface 852  
796 and thickness datasets for antarctica. *The Cryosphere* **7**, 853  
797 375–393 (2013). 854
- 798 [57] Richards, F. D., Hoggard, M. J., White, N. & Ghe- 855  
799 lichkhan, S. Quantifying the relationship between 856  
800 short-wavelength dynamic topography and thermome- 857  
801chanical structure of the upper mantle using calibrated 858  
802 parameterization of anelasticity. *Journal of Geo-*  
803 *physical Research: Solid Earth* **125**, e2019JB019062  
804 (2020). URL [https://agupubs.onlinelibrary.](https://agupubs.onlinelibrary.wiley.com/doi/abs/10.1029/2019JB019062)  
805 [wiley.com/doi/abs/10.1029/2019JB019062](https://agupubs.onlinelibrary.wiley.com/doi/abs/10.1029/2019JB019062).  
806 E2019JB019062 10.1029/2019JB019062, [https://agupubs.onlinelibrary.wiley.com/doi/pdf/](https://agupubs.onlinelibrary.wiley.com/doi/pdf/10.1029/2019JB019062)  
807 [10.1029/2019JB019062](https://agupubs.onlinelibrary.wiley.com/doi/pdf/10.1029/2019JB019062). 859
- 809 [58] Lloyd, A. J. *et al.* Decoding cenozoic tectonics in patag- 860  
810 onia, the scotia sea, and the antarctic peninsula from new 861  
811 seismic tomography. *AGUFM* **2019**, T41J–0286 (2019). 862
- 812 [59] Stocchi, P. *et al.* Mis 5e relative sea-level changes in the 863  
813 mediterranean sea: Contribution of isostatic disequilibrium. 864  
814 *Quaternary Science Reviews* **185**, 122–134 (2018). 865
- 815 [60] Golledge, N. R. *et al.* Antarctic climate and ice-sheet 866  
816 configuration during the early pliocene interglacial at 4.23 867  
817 ma. *Climate of the Past* **13** (2017). 868
- 818 [61] Shakun, J. D. *et al.* Minimal east antarctic ice sheet retreat 869  
819 onto land during the past eight million years. *Nature* **558**,  
820 284–287 (2018). 870
- 821 [62] Rogelj, J. *et al.* Paris agreement climate proposals need 871  
822 a boost to keep warming well below 2 c. *Nature* **534**,  
823 631–639 (2016). 872
- 824 [63] IPCC. *Global warming of 1.5 C. An IPCC Special Re-*  
825 *port on the impacts of global warming of 1.5 C above*  
826 *pre-industrial levels and related global greenhouse gas*  
827 *emission pathways, in the context of strengthening the*  
828 *global response to the threat of climate change, sustain-*  
829 *able development, and efforts to eradicate poverty* (2018). 873
- 830 [64] Shennan, I. Flandrian sea-level changes in the fenland. ii: 874  
831 Tendencies of sea-level movement, altitudinal changes, and 875  
832 local and regional factors. *Journal of Quaternary Science*  
833 **1**, 155–179 (1986). 876
- 834 [65] Green, J., Huber, M., Waltham, D., Buzan, J. & Wells, 877  
835 M. Explicitly modelled deep-time tidal dissipation and its 878  
836 implication for lunar history. *Earth and Planetary Science*  
837 *Letters* **461**, 46–53 (2017). 879
- 838 [66] McArthur, J., Howarth, R. & Shields, G. Strontium isotope 880  
839 stratigraphy. *The geologic time scale* **1**, 127–144 (2012). 881
- 840 [67] Bailey, T., McArthur, J., Prince, H. & Thirlwall, M. Dissol- 882  
841 ution methods for strontium isotope stratigraphy: whole 883  
842 rock analysis. *Chemical Geology* **167**, 313–319 (2000). 884
- 843 [68] Li, D., Shields-Zhou, G. A., Ling, H.-F. & Thirlwall, M. 885  
844 Dissolution methods for strontium isotope stratigraphy:  
845 Guidelines for the use of bulk carbonate and phosphorite  
846 rocks. *Chemical Geology* **290**, 133–144 (2011). 886
- 847 [69] McArthur, J. M. Recent trends in strontium isotope stratig-  
848 raphy. *Terra nova* **6**, 331–358 (1994). 887
- 849 [70] Brand, U. & Veizer, J. Chemical diagenesis of a multicom-  
850 ponent carbonate system; 1, trace elements. *Journal of*  
851 *Sedimentary Research* **50**, 1219–1236 (1980). 888
- [71] Gothmann, A. M. *et al.* Fossil corals as an archive of 889  
secular variations in seawater chemistry since the mesozoic. 890  
*Geochimica et Cosmochimica Acta* **160**, 188–208 (2015). 891
- [72] Kendall, R. A., Mitrovica, J. X. & Milne, G. A. On post- 892  
glacial sea level–ii. numerical formulation and comparative 893  
results on spherically symmetric models. *Geophysical*  
*Journal International* **161**, 679–706 (2005). 894
- [73] Peltier, W. Global glacial isostasy and the surface of the 895  
ice-age earth: the ice-5g (vm2) model and grace. *An-*  
*nual Review of Earth and Planetary Sciences* **32**, 111–149  
(2004). 896
- [74] Miller, K. G. *et al.* High tide of the warm pliocene: Im- 897  
plications of global sea level for antarctic deglaciation. 898  
*Geology* **40**, 407–410 (2012). 899
- [75] Raymo, M. E., Kozdon, R., Evans, D., Lisiecki, L. & Ford, 900  
H. L. The accuracy of mid-pliocene  $\delta^{18}O$ -based ice volume 901  
and sea level reconstructions. *Earth-Science Reviews* **177**,  
291–302 (2018). 902
- [76] Gasson, E., DeConto, R. M. & Pollard, D. Modeling the 903  
oxygen isotope composition of the antarctic ice sheet and 904  
its significance to pliocene sea level. *Geology* **44**, 827–830  
(2016). 905
- [77] Jansen, E., Fronval, T., Rack, F. & Channell, J. E. T. 906  
Pliocene-pleistocene ice rafting history and cyclicity in 907  
the nordic seas during the last 3.5 myr. *Paleoceanography*  
**15**, 709–721 (2000). 908
- [78] Bierman, P. R., Shakun, J. D., Corbett, L. B., Zimmerman, 909  
S. R. & Rood, D. H. A persistent and dynamic east green- 910  
land ice sheet over the past 7.5 million years. *Nature* **540**,  
256–260 (2016). 911
- [79] Wessel, P. & Smith, W. H. A global, self-consistent, hi- 912  
erarchical, high-resolution shoreline database. *Journal*  
*of Geophysical Research: Solid Earth* **101**, 8741–8743  
(1996). 913
- [80] Rovere, A. Paleo sea level utilities (ver 1.5) (2020). 914

# HIGHER THAN PRESENT GLOBAL MEAN SEA LEVEL RECORDED BY AN EARLY PLIOCENE INTERTIDAL UNIT IN PATAGONIA (ARGENTINA) - SUPPLEMENTARY INFORMATION -

PREPRINT, COMPILED NOVEMBER 11, 2020

Alessio Rovere<sup>1\*</sup>, Marta Pappalardo<sup>2</sup>, Sebastian Richiano<sup>3</sup>, Marina Aguirre<sup>4,5</sup>, Michael R. Sandstrom<sup>6</sup>, Paul J. Hearty<sup>7</sup>, Jacqueline Austermann<sup>6</sup>, Ignacio Castellanos<sup>5</sup>, and Maureen E. Raymo<sup>6</sup>

<sup>1</sup>MARUM - Center for Marine Environmental Sciences, University of Bremen. Leobener Str. 8., D-28359, Bremen, Germany

<sup>2</sup>Department of Earth Sciences, Università degli studi di Pisa. Via S. Maria 53, 56126, Pisa Italy

<sup>3</sup>Instituto Patagónico de Geología y Paleontología, CONICET. Bv. Almirante Brown 2915, Puerto Madryn (9120), Chubut, Argentina

<sup>4</sup>CONICET, CCT-La Plata and Universidad Nacional de La Plata. Calle 8 n.1467, B1904CMC, La Plata, Buenos Aires, Argentina

<sup>5</sup>Facultad de Ciencias Naturales y Museo, Universidad Nacional de La Plata. Calle 64 n.3, 1900 La Plata, Buenos Aires, Argentina

<sup>6</sup>Lamont Doherty Earth Observatory, Columbia University. 61 Rte 9W, Palisades, NY 10964, United States

<sup>7</sup>Department of Geological Sciences, Jackson School of Geosciences, The University of Texas at Austin. 2275 Speedway Stop C9000, Austin, Texas, United States

## 1 SUPPLEMENTARY NOTE 1: PALEO RELATIVE SEA LEVEL 2 INDICATORS IN PATAGONIA

marine/beach deposits were recognized from present-day coast-  
line inland.

**Holocene.** Holocene sea level indicators at Camarones mark the maximum sea level transgression and a sequence of regressive beach ridges. Bini et al. (2018)<sup>22</sup> reported precisely measured Holocene RSL proxies dated with <sup>14</sup>C, indicating that, between ca. 5300 and 7000 cal. yr BP, RSL was 2 to 4 m above present sea level (elevations referred to the EGM2008 Geoid).

**Marine Isotopic Stage 5e.** The Last Interglacial is also preserved in the form of relic beach ridges in the Camarones area. These were investigated and dated by different authors throughout the years<sup>9;12;10;23</sup> (Supplementary Table 1). A recent study by Pappalardo et al. (2015)<sup>9</sup> provides more precise measurements, interpretations and additional dating of the MIS 5e beach ridge complex at Camarones. According to these authors<sup>9</sup>, the beach ridges at Camarones indicate a MIS 5e paleo RSL at 7.5 +2/-3.5m above present.

**Marine Isotopic Stage 11.** At one site south of Camarones town, articulated shells from (Sample Pa 35) was dated by Schellmann and Radtke (2000)<sup>12</sup> as MIS 9 or older. U-series mollusk ages by Pappalardo et al. (2015)<sup>9</sup> confirm the attribution to MIS 11. We measured the deposits dated by these authors at 16.7 ± 0.4m above present sea level.

## SUPPLEMENTARY NOTE 2: DETAILED DESCRIPTION OF *Roadcut* AND *Caprock* UNITS AT CAMARONES

The *Roadcut* section (Supplementary Figure 1) is characterized by the bedrock (*Formación Río Chico*) outcropping from the road level up to ca.12m above it. The topmost part of the bedrock is exposed for a maximum thickness of 1.2m in the western part of the outcrop and it is shaped as a flat, gently eastward (i.e. seaward) dipping platform. All the overlying units are separated from it by a sharp erosional unconformity. Less than 1 km south of the *Roadcut*, another outcrop shows the same geological context. We refer to this as the *Caprock* outcrop

3 The study of paleo shorelines in Patagonia dates back to Charles  
4 Darwin, who was the first to provide an account of the coastal  
5 stratigraphy in the region<sup>1</sup>. Nearly a century later, the Italian ge-  
6 ologist Feruglio reported the first full account of marine terraces  
7 along the Patagonian coast (Chubut and Santa Cruz Provinces)<sup>2</sup>,  
8 that he grouped into six systems. The two uppermost systems  
9 were attributed to the to late Pliocene–early Pleistocene<sup>3</sup> based  
10 on biostratigraphic features and their high elevation (40-50 and  
11 80-95 m asl). Several studies detailed the stratigraphy, elevation  
12 and age of Holocene<sup>4;5</sup>, Pleistocene<sup>6;7;8;9;10;11;12</sup> and Pliocene-  
13 to-Miocene<sup>13;14</sup> marine and coastal deposits. The Tertiary ma-  
14 rine sediments were assigned to Miocene and Pliocene periods  
15 mostly on the basis of biostratigraphy. Several authors worked  
16 to characterize the Marine Miocene of Patagonia<sup>15;16;17</sup> and the  
17 Mio-Pliocene<sup>18</sup>. Concerning the Early Pliocene, a marine de-  
18 posit in Northern Patagonia (Rio Negro Province) yielded a  
19 fission track age of 4.41 Ma<sup>19</sup>, but this age was later considered  
20 inconsistent with biostratigraphic characteristics of the deposits  
21 and thus rejected<sup>20</sup>. Del Río et al. (2013)<sup>14</sup> dated samples of  
22 mollusks from marine deposits in Central and Southern Patag-  
23 onia, few hundreds kilometers south of our study area. The  
24 marine deposits of Cerro Laciár (300 km south of the area in-  
25 vestigated in this study, 170-185m above MSL) yielded ages of  
26 5.10 ± 0.21 Ma, and those of Cañadon Darwin (540 km south of  
27 the area investigated by this study, 65-75m above MSL) yielded  
28 ages of 5.15 ± 0.18 Ma. These two data points represent the  
29 first geochemically constrained evidence of a (Early) Pliocene  
30 transgression in the area.

31 In the coastal area around the Camarones town, the main litho-  
32 stratigraphic units are a Jurassic volcanic complex (*Complejo*  
33 *Marifil*), and Upper Paleocene sedimentary rocks (*Formación*  
34 *Río Chico*)<sup>21</sup>. According to published geological maps<sup>21</sup>, the  
35 volcanic complex is composed by reddish rhyolites, leucorhyo-  
36 lites and ignimbrites, whereas the Río Chico formation is made  
37 of mudstones, sandstones and conglomerates, often volcanoclas-  
38 tic. Along the same coastal section, fossil beach ridges and

39  
40  
41  
42  
43  
44  
45  
46  
47  
48  
49  
50  
51  
52  
53  
54  
55  
56  
57  
58  
59  
60  
61  
62  
63  
64  
65  
66  
67  
68  
69  
70  
71  
72

Supplementary Table 1: Ages of beach ridges associated to MIS 5e in the Camarones area.

Location	Author	Sample	Subsample	Age (ka)	Age uncertainty (ka)	Dating technique	
Camarones North IV	Schellmann (1998) <sup>23</sup>	Pa 30	D2412A	117	21	ESR	
			D2635	123	22	ESR	
			K2412B	139	8	ESR	
			D2550	92	9	ESR	
			D2549	99	12	ESR	
Camarones North I	Schellmann (1998) <sup>23</sup>	Pa 47c	D2665	115	9	ESR	
			D2547	117	13	ESR	
			D2546	133	15	ESR	
			D2545	137	18	ESR	
			D2548	144	19	ESR	
Camarones 12km South	Rostami et al., 2000 <sup>10</sup>	3	3-0/1	117	5	U-Series	
			3-0/2	115	9	U-Series	
			3-0/2	110	8	ESR	
			3-0/3	112	13	U-Series	
			3-0/3	114	9	ESR	
Various sites North and south of Camarones	Pappalardo et al., 2015 <sup>9</sup>	WP64A(3)	N/A	121	0.9	U-Series	
			WP65(1)	N/A	130	2.5	U-Series
			WP68(1)	N/A	131	1.1	U-Series
			WP70(B)	N/A	127	1.2	U-Series

(Supplementary Figure 2). This rests on a relative topographic high of the bedrock, which at this location is represented by the volcanic rocks pertaining to the *Complejo Marifil*, capped by a thin sedimentary unit, as thick as 1m maximum, identical to the upper part of the Cp Unit observed in the *Roadcut* section. Each overlying unit is described separately hereafter.

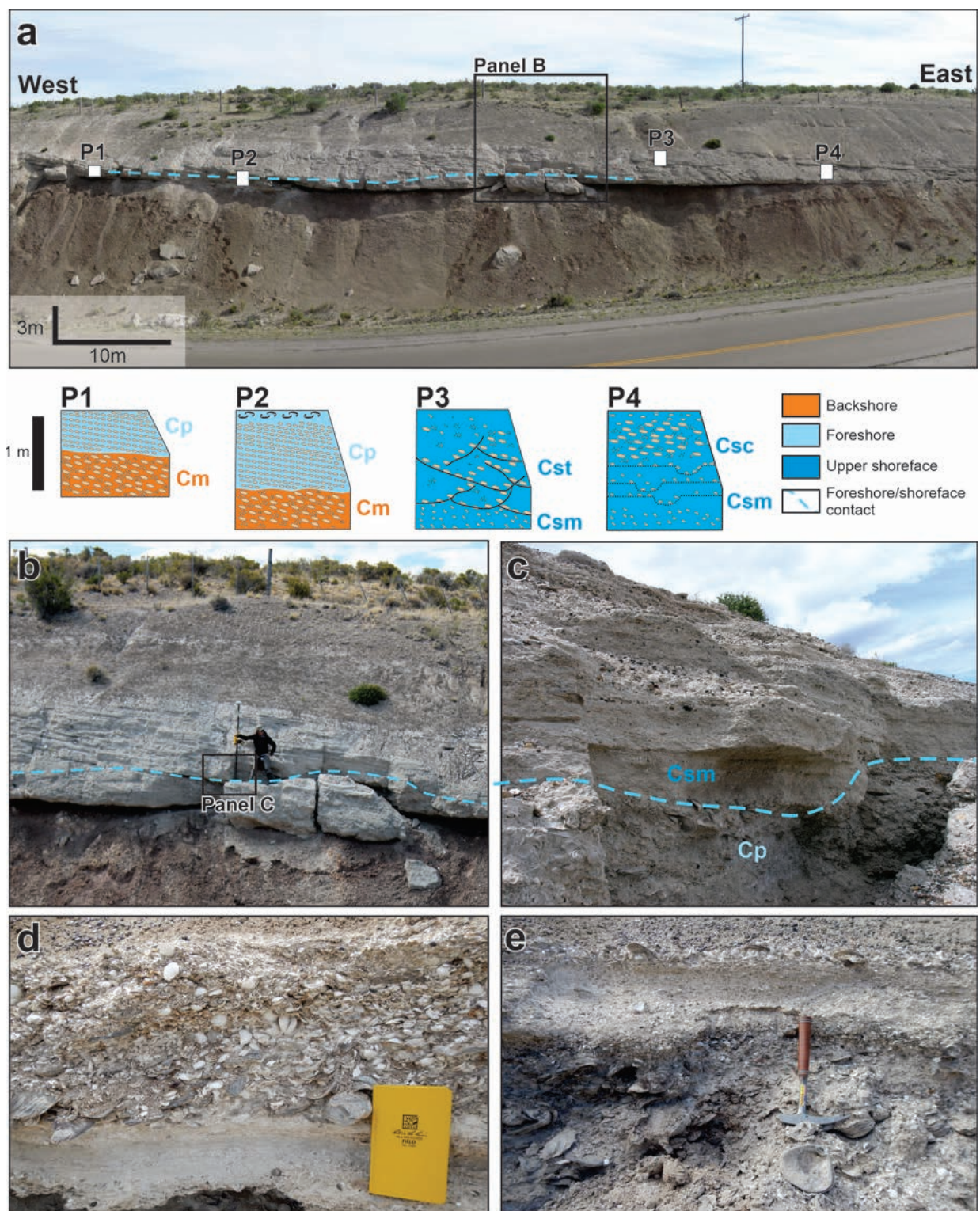
**Unit Cm.** In the western part of the section on top of the bedrock rests a basal unit (Cm). This is represented by a massive, clast-supported conglomerate with coarse rounded pebbles of different rock types. Pebbles have an imbricated, seaward dipping bedding. Faunal content is absent.

**Unit Cp.** Eastward, a finer unit (Cp) overlaps the previous one and, towards the East, unconformably rests on the bedrock. Unit Cp is composed of well-cemented fine conglomerates with rounded pebbles, mostly unbroken shells and abundant sandy matrix, displaying a low-angle planar cross-stratification. The uppermost part of Cp contains a dense faunal assemblage in the form of a shellbed, with different shell types (Supplementary Table 2) mostly intact and sometimes with paired valves (articulated), but not in living position. Only the fragmentation of Pectinids is relevant, which is expected even with minimal transport as they have a fragile shell structure. The shells in Unit Cp are characterized by different stages of preservation, depending mostly on the shell type. Big oysters (*Crassostrea* sp.), up to 15 cm in size, are frequent, mostly oriented concordant with strata dip and strike. They underwent partial dissolution, especially of their outer part, which explains the high degree of cementation of this unit. The faunal assemblage of Unit Cp is analogous to that of the Pleistocene terraces towards the coast, with notable exceptions. The absence of *Tegula atra* (cold gastropod species), together with the occurrence of bivalves of warm/warm-temperate affinity (*C. patagonica*, *D. patagonica*, *F. vilardebona*, *M. cf. isabelleana*), is the main difference relative to the Pleistocene deposits. Cp has a maximum thickness of 1m in the western part of the outcrop (stratigraphic column B, Supplementary Figure 1b).

**Unit Cs.** East of this point, the Cp unit becomes progressively thinner, and is overlapped by a finer unit (Cs) of matrix-supported sandy conglomerates. The contact between Cp and Cs is planar and displays a lateral continuity up to the midpoint of the section, East of which Cs lays directly on the bedrock. The basal part of Cs is massive (Csm) with no sedimentary structures, whereas its uppermost part, separated from Csm by a gradational contact, displays trough cross-stratification (Cst) and, more eastward, longitudinal channels (Csc).

Overall, this section represents the product of sedimentation due to a transgressive event on top of a marine platform carved in the volcanic bedrock. The sequence is fining (and thus deepening) upward. The similarities of the basal unit (Cm) with modern storm berms in the area suggest that it was formed in a backshore environment. We interpret Unit Cp as the product of sedimentation in a foreshore environment. The bedding of marine shells within this unit testifies that they have been reworked within the surf zone where sediments from upper offshore and shoreface are floated towards the beachface and from there are driven back by rip currents, producing an isorientation of single shells parallel to the current direction. The topmost Units (Csm, Cst and Csc) can be interpreted as mainly developed in middle to upper shoreface. The sedimentary structures within these units can be interpreted as the product of longitudinal currents caused by coastal drift.

109  
110  
111  
112  
113  
114  
115  
116  
117  
118  
119  
120  
121  
122  
123  
124  
125  
126  
127  
128  
129  
130  
131  
132  
133



Supplementary Figure 1: **a**) General view of the *Roadcut* section. Below the photo, four stratigraphic profiles (P1-P4) detailing the relationships between the main sedimentary facies. **Cm**: Conglomerate, massive; **Cp**: Conglomerate with low angle planar cross-stratification; **Csm**: Sandy conglomerate, massive; **Cst**: Sandy conglomerate with trough cross-stratification; **Csc**: Sandy conglomerate with longitudinal channels. **b**) Location where the elevation of unit **Cp** has been measured (the points listed in the main paper are located near the person standing on the outcrop). **c**) Detail of the contact between **Cp** (foreshore) and **Csm** (upper foreshore). **d**) and **e**) Details of the bivalve-rich horizon sampled for Sr isotopes dating.



Supplementary Table 2: Faunal assemblage in the marine deposits outcropping at the *Roadcut* section at Camarones. Most of the species recognized by Feruglio<sup>3;2</sup> and assigned to the highest terrace system (that was tentatively dated to Pliocene) were detected in the Cp Unit of the *Roadcut* section (This work). Nomenclature of the taxa has been updated as some generic or specific names do not agree with those used by Feruglio. \* indicates species with warm/warm-temperate affinity.

BIVALVIA	Feruglio <sup>3;2</sup>	This work
<i>Aulacomya atra</i> (Molina, 1782)	X	X
<i>Aequipecten tehuelchus</i> (d'Orbigny, 1842)	X	
<i>Zygochlamys patagonica</i> (King, 1832)	X	X
<i>Pectinidae</i> indet.		X
<i>Ostrea equestris</i> Say, 1834		X
<i>Ostrea puelchana</i> d'Orbigny, 1842	X	
<i>Ostrea tehuelcha</i> Feruglio	X	X
<i>Ostrea cf. tehuelcha</i> Feruglio		X
<i>Ostrea sp.</i>		X
<i>Ostrea tehuelcha</i> d'Orbigny*		X
<i>Diplodonta patagonica</i> (d'Orbigny, 1842)*		X
<i>Felaniella vilardeboana</i> (d'Orbigny, 1846)*	X	
<i>Diplodonta sp.</i>	X	
<i>Abra sp.</i>		X
<i>Mactra cf. isabellena</i> d'Orbigny, 1846*	X	X
<i>Mactra cf. patagonica</i> d'Orbigny		X
<i>Eurhomalea exalbida</i> (Dilwyn, 1817)		X
<i>Ameghinomya antiqua</i> (King, 1832)		X
<i>Pitar rostratus</i> (Philippi, 1844)	X	X
<i>Corbula patagonica</i> d'Orbigny 1845	X	X
<b>GASTROPODA</b>		
<i>Epitonium georgettinum</i> (Kiener, 1838)	X	X
<i>Trophon varians</i> (d'Orbigny, 1841)	X	X
<i>Trophon geversianus</i> (Pallas, 1774)	X	X
<i>Trophon laciniatus</i> (Martin)	X	X
<i>Adelomelon ancilla</i> (Lightfoot, 1786)	X	X
<i>Adelomelon ferussaci</i> (Donovan, 1824)		
<i>Adelomelon sp.</i>		X
<i>Odontocymbiola magellanica</i> (Gmelin, 1791)	X	X
<i>Olivancillaria auricularia</i> (Lamarck, 1811)	X	X
<i>Olivancillaria cf. carcellesi</i> Klappenbach, 1965		
<i>Buccinanops deformis</i> (P.P. King, 1832)	X	X
<i>Buccinanops cochlidium</i> (Dilwyn, 1817)	X	
<i>Buccinanops sp.</i>	X	X
<i>Siphonaria lessonii</i> Blainville, 1827		
<i>Volutidae</i> indet.	X	X

134 SUPPLEMENTARY NOTE 3: SIS AGE DETAILS.

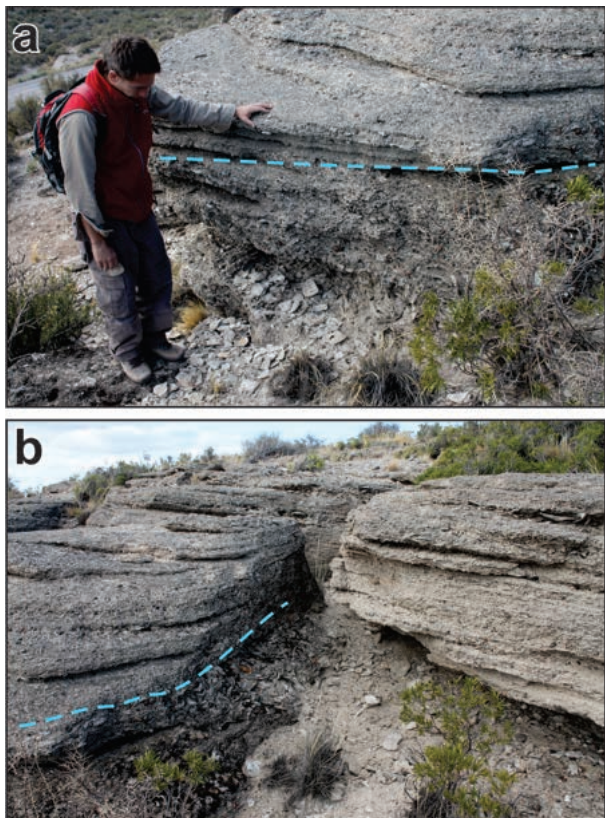
135 Details on samples and SIS analyses performed are shown here-  
 136 after, in Supplementary Figures 3 to 7. Full SIS age results are  
 137 reported in Supplementary Table 4.

138 Initial field selection criteria involved visual assessment based on  
 139 shell thickness, coloration, and diagnostic features of preservation  
 140 of original layers, and diagnostic features of preservation, including microborings, Fe and Mg staining, fragmentation  
 141 of original layers, and irregularities in structure<sup>14;24;25</sup> (Sup-  
 142 plementary Figure 4. In the laboratory, samples were slabbed,  
 143 polished and imaged using an optical microscope with CCD  
 144 camera for further inspection. and an ASPEX Express scanning  
 145 electron microscope (SEM). This preliminary screening method  
 146 helps identify locations of alteration that can be correlated with  
 147 the <sup>87</sup>Sr/<sup>86</sup>Sr leach variations and establishes the overall integrity

of preservation in each shell. A preservation scoring system was  
 established as outlined in Hearty et al. (2020)<sup>26</sup>, with optical  
 and SEM images assigned scores from "1" (no visible alteration)  
 to "3" (significant alteration observable) based on screening  
 criteria above (Supplementary Table 3).

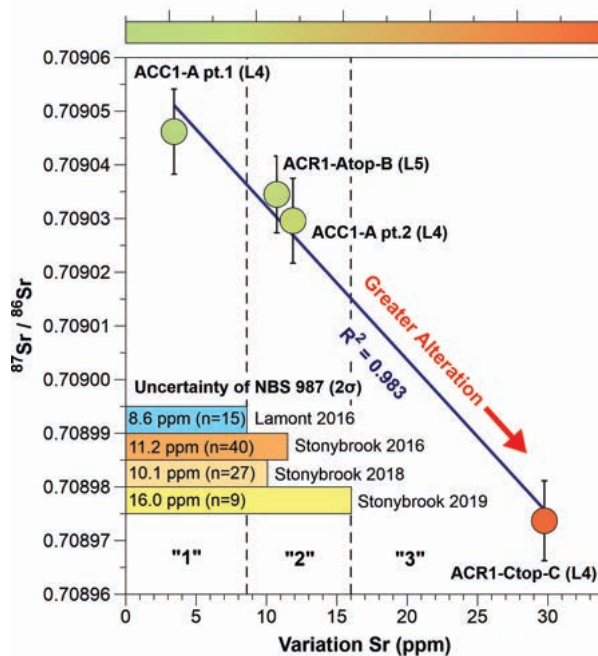
Shells were micro sampled in the best-preserved regions, pri-  
 marily through physical micro-drilling using a handheld drill  
 and the subsequent powder was homogenized by hand (except  
 in the case ACC1-A pt.2, where the shell was carefully frag-  
 mented to sand-sized grains and the Sr split was picked under a  
 microscope). Minor and trace elements were measured for three  
 samples on a Thermo iCap Q quadrupole ICP-MS at LDEO.  
 Samples were prepared and analyzed following methods similar  
 to Yu et al<sup>27</sup>. Briefly, ca.250 µg of powder was diluted to 75 ppm

148  
149  
150  
151  
152  
153  
154  
155  
156  
157  
158  
159  
160  
161



Supplementary Figure 2: **a)** and **b)** Contact between the unit Cp (lower) and Cs (higher) at the Caprock site.

along with the full dissolution splits (Supplementary Table 4 and Supplementary Figure 5). Sr was isolated and dried down using typical separation techniques with Eichon exchange resin. Following separation, 1% of Sr was removed and measured on a mass spectrometer to determine concentration. A drop of 0.05 N Phosphoric acid was added and between 150-375 ng of Sr (for each measurement) was loaded onto degassed Rhenium filaments using tantalum chloride loader.



Supplementary Figure 3: Variation of  $^{87}\text{Sr}/^{86}\text{Sr}$  within a leach set (as ppm) vs. the inner leach  $^{87}\text{Sr}/^{86}\text{Sr}$  of that shell. Sr leach variation scores are shown by dashed black line; these scores are based on the range of ppm error from seasonal long-term averages of the standard NBS 987. Green circles have low variation within leach sets (usually better preservation) and display younger SIS ages than shell ACC1-Ctop-C (red point) with high variation. This sample is excluded from the average shoreline SIS age based on high Sr variation and other screening criteria (Supplementary Table 3). Long-term uncertainty of standard NBS987 for each year/lab plotted on lower left as ppm variation.

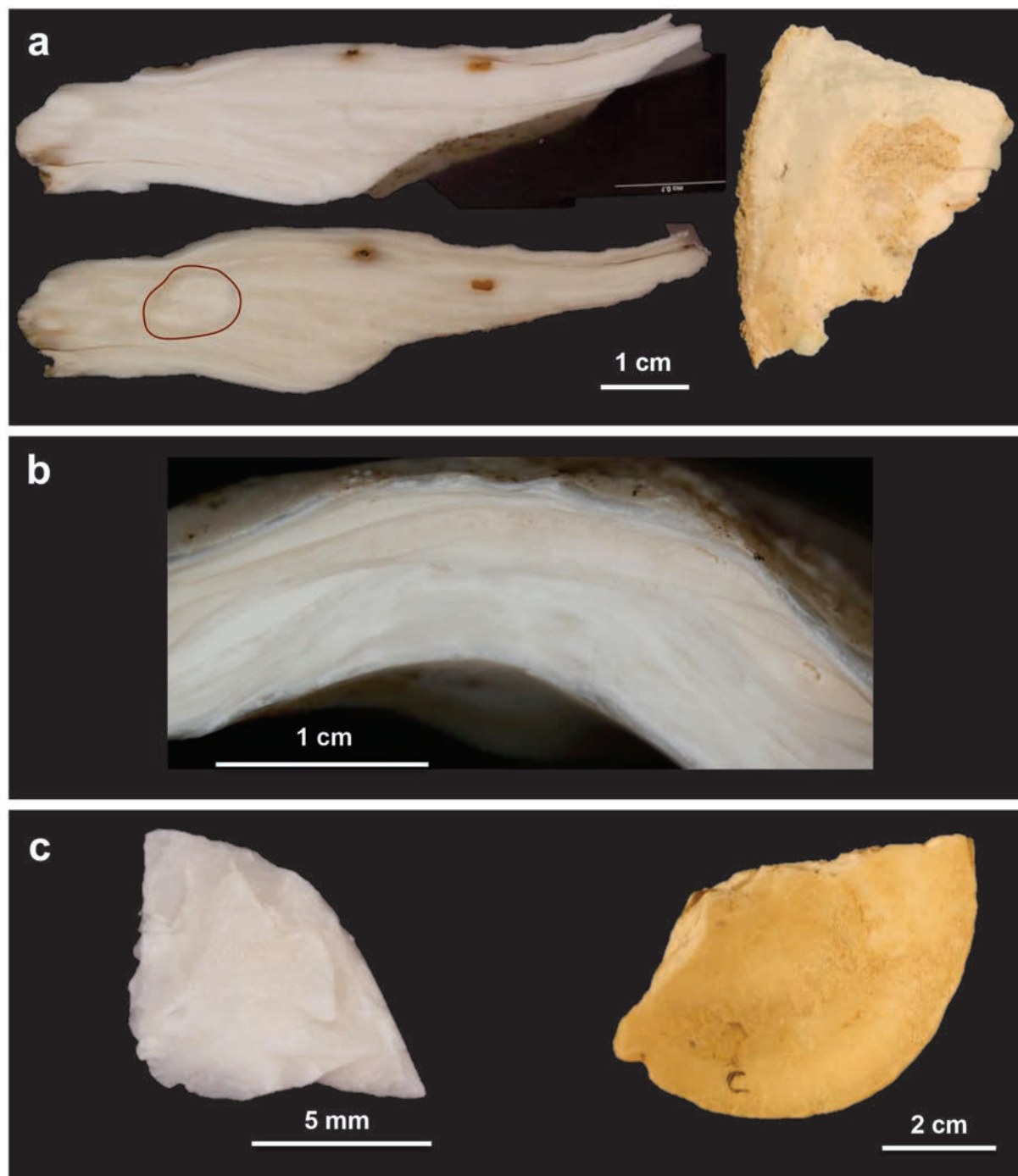
Ca (to negate matrix effects), and run alongside calibration standards covering the range of elements concentrations. The results were normalized to the in-house reference standards QC-Calcite and planktonic standard V03, the latter of which has long-term (n = 86) 2σ errors of: Sr/Ca = 1.4%, Mg/Ca = 1.3%, U/Ca = 3.0%, Ba/Ca = 1.8%, Mn/Ca = 1.2%, Al/Ca = 15.8%, Fe/Ca = 2.1% and Na/Ca = 1.3%. A Holocene bivalve (*Tridacna gigas* standard JCT-1) was run alongside the samples for comparison. An elemental scoring system was established for Mg, Mn, and Fe (Supplementary Table 3), elements thought to be indicative of diagenesis<sup>28;29;26</sup>. Scores ranged from "1" (unaltered) to "3" (altered) based on comparison to a set of Holocene corals and bivalves (for a better overview of screening methods, see Sandstrom et al. (2020)<sup>30</sup>). Sample splits were taken for Sr isotope analysis (ca. 50 mg for leach fraction, and ca. 10 mg for full dissolution).

Leaching procedures are modified from Bailey et al<sup>31</sup> (see Hearty et al., 2020<sup>26</sup>), and involve weak (ca. 0.1M) Acetic acid leaches on the powdered/fragmented shell, designed to preferentially dissolve the more loosely bound secondary  $^{87}\text{Sr}/^{86}\text{Sr}$  material before attacking the primary Sr. Typically, four to five leaches were performed per sample, each dissolving ca. 8-12 mg of carbonate (representing 16-25% of the total sample by weight). An additional split (10mg) for each sample was also fully dissolved, as an indication of the average bulk  $^{87}\text{Sr}/^{86}\text{Sr}$ . Typically, this resulted in 1400-4200 ng of Sr per leach. Only the initial (L1) and inner leaches (defined here as the dissolved 50-80% portions of each sample [i.e. L4 and L5]) were measured,

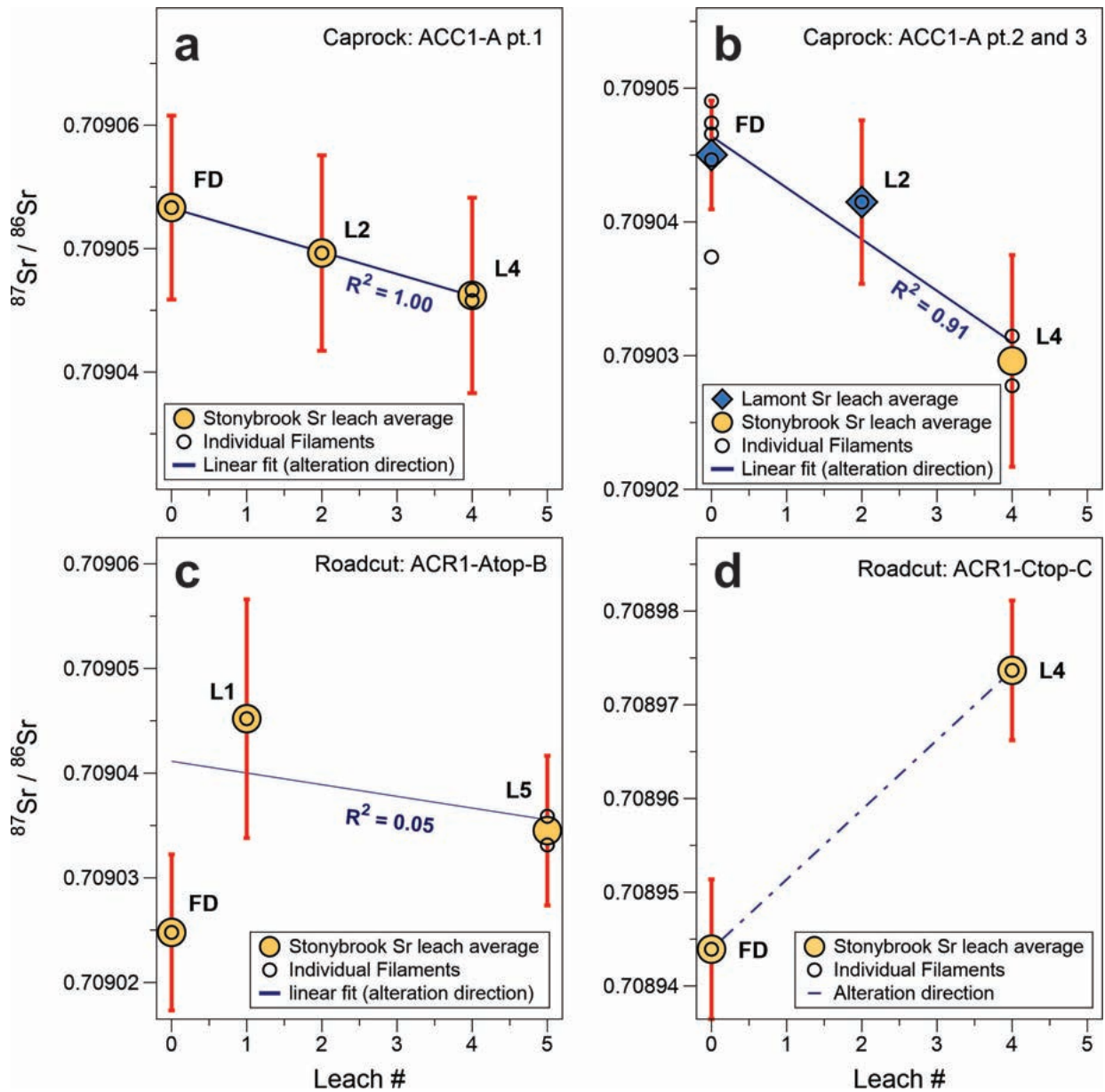
$^{87}\text{Sr}/^{86}\text{Sr}$  ratios were measured on either an IsotopX Phoenix62 Thermal Ionization Mass Spectrometer (TIMS) at Stonybrook University, or a Finnigan Triton Plus TIMS at Lamont-Doherty Earth Observatory (LDEO). Measurements at Stonybrook were conducted in a very similar manner to Gothmann et al<sup>29</sup>, with a dynamic routine measuring masses 84, 85, 86, 87, and 88 over 160 cycles for each sample. Filaments were slowly ramped up to 2.8 - 3.2 A and a temperature of ca. 1400 degrees Celsius, to achieve a beam intensity between 3-5 V on mass 88. TIMS measurements at LDEO were carried out using a static routine for 200-400 cycles with similar parameters to Stonybrook. The Sr isotope external standard NBS SRM 987 long-term instrument accuracy at the two labs was computed every season and ranged between 8.6 - 16 ppm (2σ) (Supplementary Figure 3). At Stonybrook: NBS 987 = 0.710245 ± 0.000008 (2σ; 2016, n = 40); 0.709241 ± 0.000007 (2σ; 2018, n = 27), and

214  $0.710244 \pm 0.000011$  ( $2\sigma$ ; 2019, n =9) and at LDEO: NBS 987  
215  $= 0.710238 \pm 0.000006$  ( $2\sigma$ ; 2016, n = 15). Sr isotopes were all  
216 corrected for mass fractionation based on an  $^{86}\text{Sr}/^{88}\text{Sr}$  ratio of  
217 0.1194 and normalized to the accepted NBS 987 standard value  
218  $= 0.709248$ . Sr isotope stratigraphy ages were calculated using  
219 the LOWESS version 5 curve from McArthur et al<sup>28</sup>.

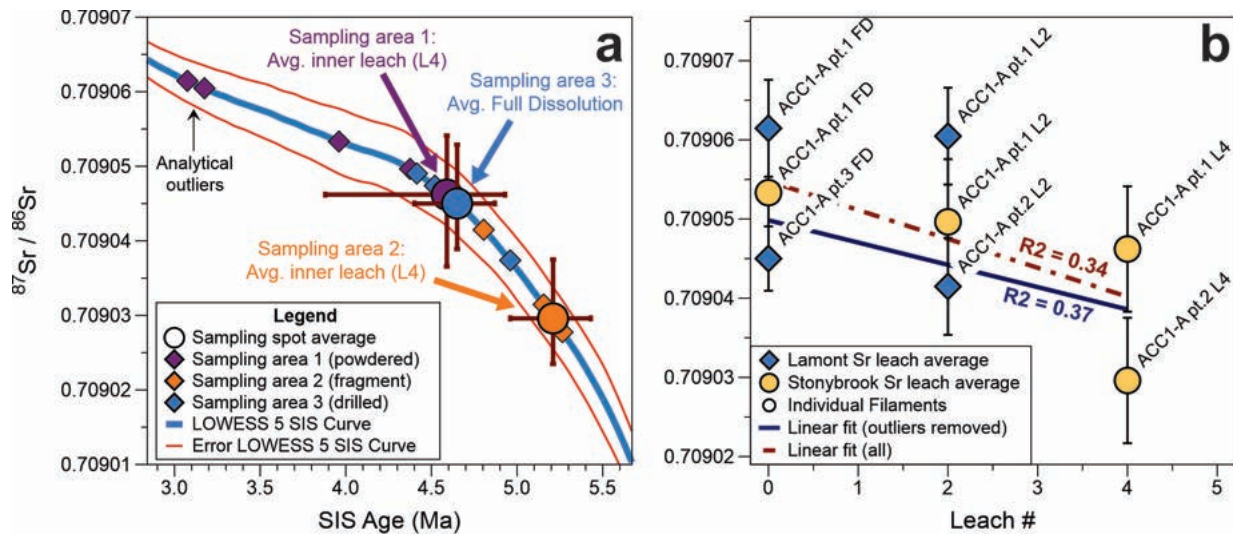
220 Sr isotope variations were calculated as ppm within leach sets (as  
221 the total range of  $^{87}\text{Sr}/^{86}\text{Sr}$  values within a leach set, multiplied  
222 by a million to read as ppm) for each sample (Supplementary  
223 Table 3). A scoring system from "1" to "3" was established based  
224 on long-term uncertainties of NBS 987, where samples with Sr  
225 isotope variations  $< 8.6\text{ppm} = 1$ , between 8.6-16 ppm = 2, and  $>$   
226 16 ppm = 3 (see Supplementary Figure 3, Supplementary Table  
227 3 and Sandstrom et al., 2020<sup>30</sup>).



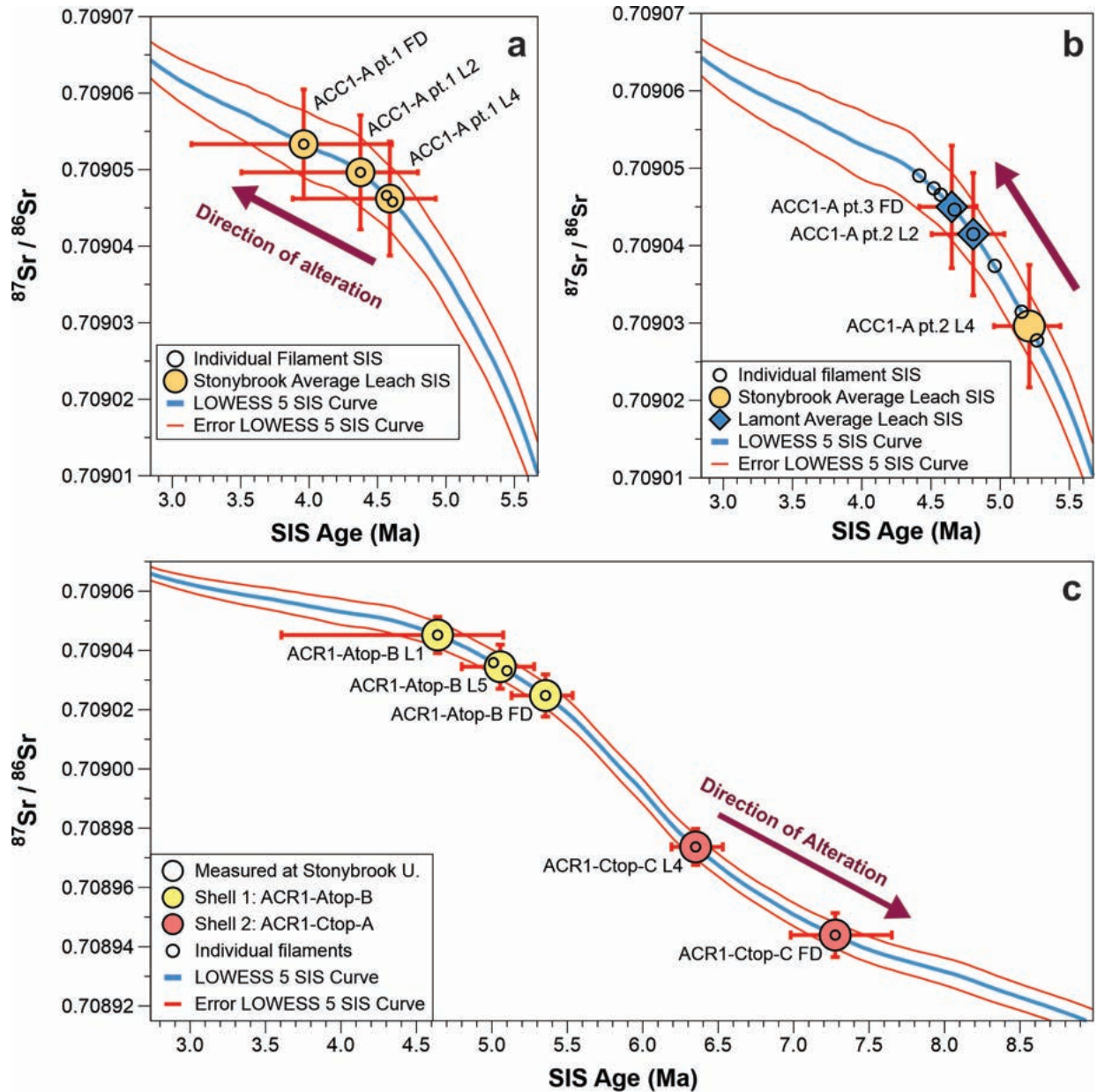
Supplementary Figure 4: Sample images. **a)** Oyster shell ACC1-A, showing slabbed x-section (top left), part 3 drill location (bottom left), and original shell fragment (right). **b)** Sample ACR1-Atop-B slabbed x-section. **c)** Shell ACR1-Ctop-C showing fragment used in Sr isotope dating (left) and partial shell collected from the field (right).



Supplementary Figure 5: Sr isotope leach set data for individual sample areas. Red error bars represent  $2\sigma$  external uncertainty of NBS987 (except for full dissolution ACC1-A pt.3 FD, which is  $2\sigma$  standard error of the mean). Linear regression lines (blue) indicate direction of alteration, with altering fluids causing the *Caprock* oyster (**a** and **b**) to appear slightly younger (more radiogenic  $^{87}\text{Sr}/^{86}\text{Sr}$ ), and the *Roadcut* samples (**c** and **d**) to appear older (alteration fluid with low  $^{87}\text{Sr}/^{86}\text{Sr}$ ). **a** and **b**) Leach set data for sample ACC1-A parts 1 and 2 showing less radioactive  $^{87}\text{Sr}/^{86}\text{Sr}$  (increased SIS age) with better preservation (L4). **c**) The inner leach lies between the initial leach and full dissolution, overlapping both within uncertainty. The leach set suggests alteration fluids cause ages to appear younger, while the full dissolution indicates the opposite. However, based upon the excellent preservation index score, the inner leach (L5) most likely reflects the original Sr isotopic ratio. **d**) The trend of significantly increasing  $^{87}\text{Sr}/^{86}\text{Sr}$  of the inner leach compared to the full dissolution indicates post-depositional alteration in this sample.



Supplementary Figure 6: **a)** Oyster shell ACC1-A (*Caprock*) detailed Sr isotopes and SIS age assignments from three different sampling locations. **b)** Leach Sr values and different TIMS machines (yellow = stonybrook, blue = Lamont). Sample splits ACC-1A pt.1 FD and L2 measured at LDEO appear to be outliers for reasons unknown [possibly turret related? as this was the first turret run?]. Repeated measurements on these same splits at SBU yielded more reliable  $^{87}\text{Sr}/^{86}\text{Sr}$  values that more closely align with other measurements from different sections of this shell, both at SBU and LDEO. Linear regression was computed for all leach averages (red) and also excluding the two outliers (blue) with similar results. There is a slight trend toward less radiogenic values for the better preserved inner leach measurements.



Supplementary Figure 7: Same data as Supplementary Figure 5. Sr isotope leach set data for individual sample areas, plotted against Lowess5 SIS curve. Red error bars represent  $2\sigma$  external uncertainty of NBS987 (except for full dissolution ACC1-A pt.3 FD, which is  $2\sigma$  standard error of the mean). Purple arrows indicate direction of alteration, with altering fluids causing the *Caprock* oyster (panels a and b) to appear younger (more radioactive  $^{87}\text{Sr}/^{86}\text{Sr}$ ), and the *Roadcut* samples (panel c) to appear older (in the case of ACR1-Ctop-C), and possibly younger in the case of ACR1-Atop-A, but no distinct trend can be assigned.

Supplementary Table 3: Elemental and diagenetic screening results of oyster samples. BDL = below detection limit. n.a. = not measured. <sup>a</sup> Jct-1 is the Holocene Tridactna standard<sup>32</sup>. <sup>b</sup> Samples used in elemental score average. <sup>c</sup> Full dissolution used for variation calculation, as L1 was not measured. <sup>d</sup> Scoring criteria outlined in Sandstrom et al. (2020)<sup>30</sup>. <sup>e</sup> See Supp. methods and Hearty et al. (2020)<sup>26</sup>. <sup>f</sup> Leach variation scores: "1" = <8.6ppm; "2" = 8.6 to 16 ppm; "3" = >16 ppm. <sup>g</sup> Samples with preservation index scores  $\geq$  "2" are considered altered and excluded.

Sample code	ACC1-A pt.1	ACR1-Atop-B	ACR1-Ctop-C	Jct-1 <sup>a</sup>
SESAR IGSN ID	IEMRS006J	IEMRS006L	IEMRS006P	N/A
Description	Caprock - Oyster	Roadcut - Oyster	Roadcut - Oyster	Holocene Tridactna
Na/Ca (mmol/mol)	8.1	9.5	11.7	19.9
Mg/Ca (mmol/mol) <sup>b</sup>	2.9	3.3	4.9	1.2
Al/Ca ( $\mu$ mol/mol)	4.6	BDL	20.4	17.2
Mn/Ca ( $\mu$ mol/mol) <sup>b</sup>	78.8	16.2	1484.7	2.6
Fe/Ca ( $\mu$ mol/mol) <sup>b</sup>	1.7	BDL	144.5	BDL
Sr/Ca (mmol/mol)	0.58	0.85	1.50	1.84
Ba/Ca ( $\mu$ mol/mol)	2.2	2.2	5.9	1.6
U/Ca (nmol/mol)	89.2	107.5	155.2	33.3
number of splits	1	2	1	3
<sup>87</sup> Sr/ <sup>86</sup> Sr leach variation (ppm)	11.88	10.73	29.75 <sup>c</sup>	n.a.
Elemental score (1-3) <sup>d</sup>	1.67	1.67	2.33	1.00
SEM score (1-3) <sup>e</sup>	2	n.d.	2	n.a.
Optical score (1-3) <sup>e</sup>	2	1	2	1
<sup>87</sup> Sr/ <sup>87</sup> Sr variation score (1-3) <sup>f</sup>	2	2	3	n.a.
<b>Preservation Index Score<sup>g</sup> (average of all scores: 1-3)</b>	<b>1.92</b>	<b>1.56</b>	<b>2.33</b>	<b>1.00</b>



Supplementary Table 4:  $^{87}\text{Sr}/^{86}\text{Sr}$  results and Sr isotope stratigraphy ages for Caprock and Roadcut outcrops. <sup>a</sup> Inner leach Sr isotope values for sample; <sup>b</sup> Sample leaches excluded based on analytical or diagenetic criteria; <sup>c</sup> Sample excluded from shoreline age based on significant diagenesis (see Table S3); <sup>d</sup> Uncertainty based on  $2\sigma$ SEM; <sup>e</sup> Sample variation is calculated as the difference between the initial leach [or full dissolution] and last leach, multiplied by one million (ppm); <sup>f</sup> Average of inner leaches on samples that passed screening criteria: ACC1-A pts. 1 and 2, and ACR1-Atop-B; <sup>g</sup> Uncertainty based on combined analytical [ $2\sigma$ SEM] and SIS curve [LOWESS 5] errors.

Sample Name	TIMS Lab	Leach ID	Nb. filaments	$^{87}\text{Sr}/^{86}\text{Sr}$ (measured)	$^{87}\text{Sr}/^{86}\text{Sr}$ (normalized to NBS97)	$2\sigma$ external uncertainty	Mean SIS Age (Ma)	Maximum SIS Age (Ma)	Minimum SIS Age (Ma)	Uncorrected SIS Age (Ma)
<b>Average <math>^{87}\text{Sr}/^{86}\text{Sr}</math> by Leach</b>										
<b>Caprock</b>										
ACC1-A pt.1 FD	SBU	FD	1	0.7090465	0.7090533	0.0000075	3.960	4.605	3.140	4.58
ACC1-A pt.1 L2	SBU	L2	1	0.7090462	0.7090496	0.0000079	4.375	4.795	3.505	4.59
ACC1-A pt.1 L4 <sup>a</sup>	SBU	L4	2	0.7090427	0.7090462	0.0000079	4.590	4.925	3.880	4.76
ACC1-A pt.1 FD <sup>b</sup>	LDEO	FD	1	0.7090509	0.7090615	0.0000061	3.075	3.745	2.635	4.27
ACC1-A pt.1 L2 <sup>b</sup>	LDEO	L2	1	0.7090499	0.7090605	0.0000061	3.175	3.855	2.695	4.36
ACC1-A pt.2 L2	LDEO	L2	1	0.7090309	0.7090415	0.0000061	4.805	5.030	4.505	5.17
ACC1-A pt.2 L4 <sup>a</sup>	SBU	L4	2	0.7090261	0.7090296	0.0000079	5.210	5.435	4.955	5.32
ACC1-A pt.3 FD	LDEO	FD	5	0.7090345	0.7090344	0.0000041 <sup>d</sup>	4.650	4.415	4.830	5.055
<b>Roadcut</b>										
ACR1-Atop-B FD	SBU	FD	1	0.7090180	0.7090248	0.0000075	5.355	5.535	5.130	5.52
ACR1-Atop-B L1	SBU	L1	1	0.7090409	0.7090452	0.0000114	4.640	5.075	3.605	4.83
ACR1-Atop-B L5 <sup>a</sup>	SBU	L5	2	0.7090279	0.7090345	0.0000072	5.055	5.280	4.800	5.27
ACR1-Ctop-C FD	SBU	FD	1	0.7089371	0.7089439	0.0000075	7.275	7.650	6.980	7.62
ACR1-Ctop-C L4 <sup>a,c</sup>	SBU	L4	1	0.7089668	0.7089737	0.0000075	6.350	6.530	6.190	6.52
<b>Average Shoreline SIS Age</b>										
Average of screened inner leaches <sup>f</sup>	SBU	L4, L5	6	0.7090322	0.7090368	0.0000064 <sup>d</sup>	4.98	5.225 <sup>e</sup>	4.685 <sup>e</sup>	5.13

228 REFERENCES

- 229 [1] Darwin, C. *Geological observations on South America: Being the third part of the geology of the voyage of the*  
 230 *Beagle, under the command of Capt. Fitzroy, RN during*  
 231 *the years 1832 to 1836* (Smith, Elder and Company, 65,  
 232 Cornhill., 1846).  
 233
- 234 [2] Feruglio, E. *I terrazzi marini della Patagonia* (Cooperativa  
 235 Tip. Edit. Paolo Galeati, 1933).
- 236 [3] Feruglio, E. *Descripción geológica de la Patagonia*, vol. 1  
 237 (Impr. y Casa Editora "Coni", 1949).
- 238 [4] Schellmann, G. & Radtke, U. Coastal terraces and  
 239 holocene sea-level changes along the patagonian atlantic  
 240 coast. *Journal of Coastal Research* 983–996 (2003).
- 241 [5] Zanchetta, G. *et al.* Middle-to late-holocene relative sea-  
 242 level changes at puerto deseado (patagonia, argentina). *The*  
 243 *Holocene* **24**, 307–317 (2014).
- 244 [6] Bini, M. *et al.* Markers of palaeo sea-level in rocky coasts  
 245 of patagonia (argentina). *Rendiconti Online della Società*  
 246 *Geologica Italiana* **20**, 10–14 (2013).
- 247 [7] Fucks, E. *et al.* Influence of quaternary sea level changes in  
 248 the littoral of chubut, argentina. *Journal of South American*  
 249 *Earth Sciences* **88**, 589–598 (2018).
- 250 [8] Pappalardo, M. *et al.* Challenges in relative sea-level  
 251 change assessment highlighted through a case study: The  
 252 central coast of atlantic patagonia. *Global and Planetary*  
 253 *Change* **182**, 103008 (2019).
- 254 [9] Pappalardo, M. *et al.* Coastal landscape evolution and  
 255 sea-level change: A case study from central patagonia  
 256 (argentina). *Zeitschrift für Geomorphologie* **59**, 145–172  
 257 (2015).
- 258 [10] Rostami, K., Peltier, W. & Mangini, A. Quaternary marine  
 259 terraces, sea-level changes and uplift history of patago-  
 260 nia, argentina: comparisons with predictions of the ice-4g  
 261 (vm2) model of the global process of glacial isostatic ad-  
 262 justment. *Quaternary Science Reviews* **19**, 1495–1525  
 263 (2000).
- 264 [11] Pedoja, K. *et al.* Uplift of quaternary shorelines in eastern  
 265 patagonia: Darwin revisited. *Geomorphology* **127**, 121–  
 266 142 (2011).
- 267 [12] Schellmann, G. & Radtke, U. ESR dating stratigraphically  
 268 well-constrained marine terraces along the patagonian at-  
 269 lantic coast (argentina). *Quaternary International* **68**, 261–  
 270 273 (2000).
- 271 [13] Rutter, N. *et al.* Correlation and dating of quaternary  
 272 littoral zones along the patagonian coast, argentina. *Qua-*  
 273 *ternary Science Reviews* **8**, 213–234 (1989).
- 274 [14] Del Río, C., Griffin, M., McArthur, J., Martínez, S. &  
 275 Thirlwall, M. Evidence for early pliocene and late miocene  
 276 transgressions in southern patagonia (argentina): 87sr/86sr  
 277 ages of the pectinid "chlamys" actinodes (sowerby). *Jour-*  
 278 *nal of South American Earth Sciences* **47** (2013).
- 279 [15] del Río, C. J., Martínez, S. A. & Scasso, R. A. Nature  
 280 and origin of spectacular marine miocene shell beds of  
 281 northeastern patagonia (argentina): Paleocological and  
 282 bathymetric significance. *Palaios* **16**, 3–25 (2001).
- [16] Dozo, M. T. *et al.* Late miocene continental biota in north-  
 283 eastern patagonia (península valdés, chubut, argentina).  
 284 *Palaeogeography, Palaeoclimatology, Palaeoecology* **297**,  
 285 100–109 (2010).  
 286
- [17] Farinati, E. & Zavala, C. Trace fossils on shelly substrate.  
 287 an example from the miocene of patagonia, argentina. *Acta*  
 288 *Geologica Hispanica* **37**, 29–36 (2002).  
 289
- [18] del Río, C. J. Tertiary marine molluscan assemblages of  
 290 eastern patagonia (argentina): a biostratigraphic analysis.  
 291 *Journal of Paleontology* **78**, 1097–1122 (2004).  
 292
- [19] Bigazzi, G., Bonadonna, F., Leone, G. & Zanchetta, G.  
 293 Primeros datos geoquímicos y geocronológicos a partir  
 294 de algunas cineritas del area bonarense (1995).  
 295
- [20] Farinati, E. A. & Zavala, C. A. Asociaciones de  
 296 megafósiles de invertebrados en el neógeno atlántico de la  
 297 patagonia argentina (2005).  
 298
- [21] Lema, H. A. *et al.* Hoja geológica 4566-ii y iv camarones  
 299 (2001).  
 300
- [22] Bini, M. *et al.* Mid-holocene relative sea-level changes  
 301 along atlantic patagonia: new data from camarones, chubut,  
 302 argentina. *The Holocene* **28**, 56–64 (2018).  
 303
- [23] Schellmann, G. *Jungkänozoische Landschaftsgeschichte*  
 304 *Patagoniens (Argentinien): andine Vorlandvergletscherun-*  
 305 *gen, Talentwicklung und marine Terrassen* (1. Auflage,  
 306 Essen: Klartext, 1998, 1998).  
 307
- [24] McArthur, J. M. Recent trends in strontium isotope stratig-  
 308 raphy. *Terra nova* **6**, 331–358 (1994).  
 309
- [25] Cochran, J. K. *et al.* Effect of diagenesis on the sr, o, and  
 310 c isotope composition of late cretaceous mollusks from  
 311 the western interior seaway of north america. *American*  
 312 *Journal of Science* **310**, 69–88 (2010).  
 313
- [26] Hearty, P. J. *et al.* Pliocene-pleistocene stratigraphy and  
 314 sea-level estimates, republic of south africa with implica-  
 315 tions for a 400 ppmv co2 world. *Paleoceanography and*  
 316 *Paleoclimatology* **n/a**, n/a (2020).  
 317
- [27] Yu, J., Day, J., Greaves, M. & Elderfield, H. Determina-  
 318 tion of multiple element/calcium ratios in foraminiferal  
 319 calcite by quadrupole icp-ms. *Geochemistry, Geophysics,*  
 320 *Geosystems* **6** (2005).  
 321
- [28] McArthur, J., Howarth, R. & Shields, G. Strontium isotope  
 322 stratigraphy. *The geologic time scale* **1**, 127–144 (2012).  
 323
- [29] Gothmann, A. M. *et al.* Fossil corals as an archive of  
 324 secular variations in seawater chemistry since the mesozoic.  
 325 *Geochimica et Cosmochimica Acta* **160**, 188–208 (2015).  
 326
- [30] Sandstrom, M. R. *et al.* Age constraints on surface  
 327 deformation recorded by fossil shorelines at Cape  
 328 Range, Western Australia. *GSA Bulletin* (2020). URL  
 329 <https://doi.org/10.1130/B35564.1>. <https://pubs.geoscienceworld.org/gsabulletin/article-pdf/doi/10.1130/B35564.1/5135376/b35564.pdf>.  
 330  
 331  
 332  
 333
- [31] Bailey, T., McArthur, J., Prince, H. & Thirlwall, M. Disso-  
 334 lution methods for strontium isotope stratigraphy: whole  
 335 rock analysis. *Chemical Geology* **167**, 313–319 (2000).  
 336

- 337 [32] Watanabe, T., Suzuki, A., Kawahata, H., Kan, H. & Ogawa,  
338 S. A 60-year isotopic record from a mid-holocene fossil  
339 giant clam (*tridacna gigas*) in the ryukyu islands: physio-  
340 logical and paleoclimatic implications. *Palaeogeography,*  
341 *Palaeoclimatology, Palaeoecology* **212**, 343–354 (2004).